



Since January 2020 Elsevier has created a COVID-19 resource centre with free information in English and Mandarin on the novel coronavirus COVID-19. The COVID-19 resource centre is hosted on Elsevier Connect, the company's public news and information website.

Elsevier hereby grants permission to make all its COVID-19-related research that is available on the COVID-19 resource centre - including this research content - immediately available in PubMed Central and other publicly funded repositories, such as the WHO COVID database with rights for unrestricted research re-use and analyses in any form or by any means with acknowledgement of the original source. These permissions are granted for free by Elsevier for as long as the COVID-19 resource centre remains active.



Xuanfei Baidu Decoction reduces acute lung injury by regulating infiltration of neutrophils and macrophages *via* PD-1/IL17A pathway

Yuying Wang^{a,b}, Xi Wang^{a,b}, Yixuan Li^{a,b}, Zhifeng Xue^{a,b}, Rui Shao^{a,b}, Lin Li^{a,b,c}, Yan Zhu^{a,b}, Han Zhang^{a,b,c,*}, Jian Yang^{a,b,*}

^a State Key Laboratory of component-based Chinese Medicine, Tianjin University of Traditional Chinese Medicine, Tianjin 301617, China

^b Institute of Traditional Chinese Medicine, Tianjin University of Traditional Chinese Medicine, Tianjin 301617, China

^c Key Laboratory of Pharmacology of Traditional Chinese Medical Formulae, Tianjin University of Traditional Chinese Medicine, Ministry of Education, Tianjin 301617, China

ARTICLE INFO

Keywords:

COVID-19

Xuanfei Baidu Decoction

Acute lung injury

PD-1/IL17A pathway

Systematic network pharmacological analysis

Chemical compounds studied in this article:

Glycyrrhizic acid (PubChem CID: 14982)

Naringin (PubChem CID: 442428)

Acteoside (PubChem CID: 5281800)

Liquiritin (PubChem CID: 503737)

Polydatin (PubChem CID: 5281718)

Hastatoside (PubChem CID: 92043450)

Verbenalin (PubChem CID: 73467)

Amygdalin (PubChem CID: 656516)

Sinapine (PubChem CID: 5280385)

Ephedrine (PubChem CID: 9294)

ABSTRACT

The pathogenic hyper-inflammatory response has been revealed as the major cause of the severity and death of the Corona Virus Disease 2019 (COVID-19). Xuanfei Baidu Decoction (XFBD) as one of the “three medicines and three prescriptions” for the clinically effective treatment of COVID-19 in China, shows unique advantages in the control of symptomatic transition from moderate to severe disease states. However, the roles of XFBD to against hyper-inflammatory response and its mechanism remain unclear. Here, we established acute lung injury (ALI) model induced by lipopolysaccharide (LPS), presenting a hyperinflammatory process to explore the pharmacodynamic effect and molecular mechanism of XFBD on ALI. The *in vitro* experiments demonstrated that XFBD inhibited the secretion of IL-6 and TNF- α and iNOS activity in LPS-stimulated RAW264.7 macrophages. *In vivo*, we confirmed that XFBD improved pulmonary injury *via* down-regulating the expression of proinflammatory cytokines such as IL-6, TNF- α and IL-1 β as well as macrophages and neutrophils infiltration in LPS-induced ALI mice. Mechanically, we revealed that XFBD treated LPS-induced acute lung injury through PD-1/IL17A pathway which regulates the infiltration of neutrophils and macrophages. Additionally, one major compound from XFBD, *i.e.* glycyrrhizic acid, shows a high binding affinity with IL17A. In conclusion, we demonstrated the therapeutic effects of XFBD, which provides the immune foundations of XFBD and fatherly support its clinical applications.

1. Introduction

The Coronavirus Disease 2019 (COVID-19), caused by the severe acute respiratory syndrome type 2 Coronavirus (SARS-CoV-2) poses a major threat to global public health and the economy. There is increasing evidence that inflammatory syndrome caused by over-activation of the immune system contributes to the severity of COVID-19 [1]. The virus releases damage associated molecular patterns (DAMPs), which are recognized by adjacent epithelial cells, endothelial cells, and

alveolar macrophages, initiating the proinflammatory signaling cascade, then the cytokines and chemokines attract macrophages, neutrophils, and T cells to the site of infection, where they release more factors to set up pro-inflammatory feedback loops that aggravate cellular damage [2,3].

COVID-19 patients range from asymptomatic or mild upper respiratory disease to severe viral pneumonia, which can progress to cytokine storms, acute respiratory distress syndrome (ARDS) and death, almost all patients with severe COVID-19 have bilateral lung involvement, and

Abbreviation: COVID-19, coronavirus disease 2019; SARS-CoV-2, severe acute respiratory syndrome type 2 Coronavirus; ACE2, angiotensin-converting enzyme 2; ALI, acute lung injury; ARDS, acute respiratory distress syndrome; XFBD, Xuanfei Baidu Decoction; LPS, lipopolysaccharide; DAD, diffuse alveolar damage; TCM, Traditional Chinese Medicine; BALF, bronchoalveolar lavage fluid; WBP, Whole Body Plethysmography; WBC, white blood cell; PB, peripheral blood.; IL17A, interleukin 17A; PD-1, programmed death 1 protein; TIMP1, tissue inhibitor of metalloproteinases 1; MUC5AC, mucin-5 subtype AC; CCL2, C-C motif chemokine ligand 2; CXCL10, C-X-C motif chemokine ligand 10; MPO, myeloperoxidase; PMNE, neutrophil elastase.

* Corresponding authors at: State Key Laboratory of component-based Chinese Medicine, Tianjin University of Traditional Chinese Medicine, Tianjin 301617, China.

E-mail addresses: zhanghan0023@126.com (H. Zhang), yang.j2017@tjutcm.edu.cn (J. Yang).

<https://doi.org/10.1016/j.phrs.2022.106083>

Received 4 November 2021; Received in revised form 29 December 2021; Accepted 10 January 2022

Available online 13 January 2022

1043-6618/© 2022 Elsevier Ltd. All rights reserved.

15–40% of COVID-19 patients will develop ARDS [4]. Histologically, acute lung injury (ALI) is defined as diffuse alveolar damage (DAD), which was mainly divided into three stages: acute or exudative stage (fluid accumulation in lung tissue, pulmonary edema phenomenon); Tissue or proliferative stage; Chronic or fibrotic stage [5]. DAD has been reported in both SARS-CoV-2-infected human and non-human primates [6]. During the development of ALI, systemic inflammatory reactions occur. Neutrophils and macrophages accumulate in the lungs and generate a large number of inflammatory signals, leading to pulmonary edema and injury of alveolar epithelial cells and vascular endothelial cells [7,8]. Trying to address excessive inflammation is an effective therapeutic strategy for controlling ALI and COVID-19. Lipopolysaccharide (LPS) is an outer membrane component of gram-negative bacteria, cause severe inflammatory responses. In the LPS-induced ALI model, mice showed similar pathological damage to COVID-19 [9].

The mechanisms of ALI were partially revealed. The pattern recognition receptor Toll-like receptor 4 (TLR4) was activated, which activated Janus kinase 2 (JAK2) [10], protein kinase B (PKB/Akt) [11], extracellular signal-associated kinase (ERK1/2) [12], spleen tyrosine kinase (SYK) and interleukin-1 receptor-associated kinase 1 (IRAK1) [13], and myeloid differentiation factor 88 (MyD88) [14], further promoting phosphorylation of signal transducer and activator of transcription 3 (STAT3) and nuclear translocation of nuclear factor kappa B subunit 1 (NF- κ B), and these changes up-regulated the expression of genes involved in inflammatory response like myeloperoxidase (MPO), monocyte chemoattractant protein 1 (MCP-1/CCL2), macrophage inflammatory protein-1 alpha (MIP-1a), interleukins (IL-6, IL-8, IL-1 β), tumor necrosis factor (TNF) and granulocyte-macrophage colony-stimulating factor (GM-CSF). Moreover, the importance of IL17A in ALI was discovered. For MERS-CoV, SARS-CoV, and SARS-CoV-2 infections, the severity of the disease was positively correlated with IL17A levels, and the overproduction of IL17A observed in ALI patients had been reproduced in LPS-induced ALI mice [15]. IL17A is derived from a variety of immune and inflammatory cells, including T lymphocytes, NK cells, monocytes/macrophages, neutrophils, and mast cells, fibroblasts and epithelial cells also contribute to the increase of IL17A [16,17]. On the other hand, IL17A receptors are commonly expressed on a variety of cell surfaces, including monocytes/macrophages, neutrophils, epithelial cells and fibroblasts [17,18].

In the process of fighting the epidemic, traditional Chinese medicine (TCM) received high attentions. The National Health Commission has successively released ten editions of COVID-19 Diagnosis and Treatment Protocol, all of which recommended TCM treatments. XFBD is one of the “three medicines and three prescriptions” of TCM in the treatment of COVID-19 patients. It has obvious effects in shortening the disappearance time of clinical symptoms, the time of returning to normal body temperature, the average length of hospital stay, etc., and shows unique advantages in blocking the transition from mild to severe type [19]. There is a recent report that XFBD prescription cured a severe COVID-19 patient, which has the effects of inhibiting viral infection, reducing inflammatory factors and promoting the absorption of lung inflammation [20]. Network pharmacological analysis suggested that XFBD plays a role in balancing the immune inflammatory responses [21]. However, the underlying mechanism regulating immune responses by XFBD still remains unknown.

In our study, a series of experimental methods including μ CT, WBP, H&E staining, qRT-PCR, IHC and ELISA assays were performed to evaluate the immunoregulation effects of XFBD in ALI. Transcriptomics and network pharmacology were used to explore the underlying mechanism, monoclonal antibody blocking experiment, molecular docking and SPR analysis were also performed to clarify this mechanism. Our results revealed the underlying immunological mechanism of XFBD, providing the research foundation for its clinical applications.

2. Materials and methods

2.1. Chemicals and reagents

XFBD was provided by Tianjin Modern TCM Innovation Center (TRT 200302). LPS was purchased from Sigma-Aldrich (Shanghai, China). Dexamethasone was purchased from Yuanye Bio (Shanghai, China). Anti-TNF- α antibody, anti-F4/80 antibody, anti-Neutrophil Elastase antibody, anti-IL17A antibody and Alexa Fluor®488-conjugated goat anti-Rat IgG were purchased from Abcam (Cambridge, MA, USA). Recombinant human IL17A was purchased from R&D systems (Minneapolis, USA). IL-17A monoclonal antibody (IL17A mAb) and mouse IgG1 kappa isotype control (IgG1K) were purchased from eBioscience (San Diego, California, USA). Anti-PD-1 antibody was purchased from Proteintech (Wuhan, China). HRP-conjugated goat anti-rabbit IgG was purchased from ZSGB-BIO (Beijing, China). Enzyme linked immunosorbent assay kits of TNF- α was purchased from ZCI BiO (Shanghai, China). glycyrrhizic acid, DMSO, RIPA lysis, BCA Protein Assay Reagent Kit and PMSF were purchased from Solarbio (Beijing, China). DAB substrate kit was purchased from Boster Biological (Wuhan, China). The myeloperoxidase (MPO) detection kit was purchased from Nanjing Jiancheng Bioengineering Institute.

2.2. Cell culture and TNF- α detection

RAW264.7 macrophages were maintained in Dulbecco's Modified Eagle's Medium (DMEM, Gibco) supplemented with 10% heat-inactivated FBS, 1% penicillin and streptomycin, followed by incubation at 37 °C in a humidified atmosphere containing 5% CO₂.

The RAW264.7 cells were seeded into 96-well plates at a density of 5×10^4 cells/mL, after 24 h incubation, the culture medium was replaced with serum-free medium for another 12 h. Then cells were treated with LPS (500 ng/mL) and XFBD (0, 10, 25, 50, 100, 200 μ g/mL) for 12 h. Cells were fixed with 4% paraformaldehyde and permeabilized with 0.5% Triton X-100 for 10 min followed by treated with 2% BSA for 1.5 h at 37 °C. Cells were incubated with the TNF- α primary antibody (1:200, Abcam, #ab9739) overnight at 4 °C and stained with secondary antibody and Hoechst 33342 for 1.5 h at room temperature. Visual images and quantitative analysis were obtained with Operetta High Content Analysis (HCA) System (PerkinElmer, Boston, MA, USA). At least 5 random microscopic fields were selected.

2.3. Acute Lung Injury (ALI) model

SPF healthy male C57BL/6 mice (20–23 g) were provided by SPF (Beijing) Biotechnology Co., LTD. (Certificate number: SCXK Jing 2017-0005). The mice were kept in Tianjin International Joint Academy of Biotechnology and Medicine at a temperature of 19–25 °C and relative humidity of 40–60%. 6 mice in each cage, they were given regular feed and free water. After 1 week of adaptive feeding, the mice were randomly divided into sham group (Sham), model group (LPS), dexamethasone group (Dex, 5 mg/kg), XFBD low dose group (XFBD-L, 4.6 g/kg) and XFBD high dose group (XFBD-H, 9.2 g/kg) (n = 6). The dosage of XFBD-L used in mice was converted from clinical dosage with the following formula:

$$\text{The dosage of XFBD-L} = 238 \text{ g} \times 12.6\% \times 9.1/60 \text{ kg}$$

The clinical raw drug dosage was 238 g/ person/day, and the ointment yield rate was 12.6%. The average body weight of normal adults was 60 kg, and the equivalent dose ratio of human and mouse was 9.1.

After anesthesia with tribromoethanol, mice received lipopolysaccharide (4 mg/kg) in saline or the same volume of saline. XFBD was given half an hour before LPS infusion and once a day thereafter. All experiments were reviewed and approved by the Institutional Animal Care and Use Committee at the Tianjin International Joint Academy of

Biotechnology and Medicine and were carried out under the Guidelines for Animal Experiments of Tianjin University of TCM (Animal Ethics License Number: TJAB-JY-2019-002).

2.4. Micro CT scanning (μ CT)

Mice were scanned with a μ CT scanner (Micro-CT QuantumFX μ CT Software, PerkinElmer, American). Each mouse underwent only one CT imaging session and was thereafter euthanized. LPS-treated mice were scanned on the 2nd day and 5th day following LPS. The mice in sham group were also scanned. The mice were positioned in the scanner and a μ CT scan was acquired of the chest for anatomic localization and attenuation correction using the following parameters: 90 kV, 160 mA and 40 mm. The X-ray system uses a 5 mm micro focusing tube with a spot size and a conical beam geometry to generate X-rays. The maximum width of the image field is 68 mm and the voxel size is $35 \times 35 \times 35$ mm.

2.5. Lung function test

Lung function is one of the more intuitive and objective indicators to reflect the occurrence and development of respiratory diseases, and Whole Body Plethysmography (WBP) is often used to evaluate drug efficacy in animal models with respiratory diseases due to its advantages of non-invasive, simple operation and simultaneous detection [22]. Sheahan et al. reported WBP results in a comparative study of antiviral combination therapy with MERS-CoV [23]. Briefly, the lung function of each mouse was examined using the Emka WBP lung function test system on the 2nd day and 5th day after LPS infusion. Before the pulmonary function test, make sure that the four tracer cavities are well connected and sealed. 10 mL air is injected to correct it. The specific parameters are as follows: input "0" at Low value, input "- 100" at High value, input "mL/s" at Unit, and the calibration range is 3500–5000. After all calibration, the mice were put into the animal volume tracing chambers in batches and then start the test. The system automatically detects each indicator every 10 s, and information collection (iox2 2.9.4.32) was stopped after 20 min.

2.6. Histopathological observation

The lung tissues that fixed in 4% paraformaldehyde fixing solution were dehydrated, embedded in paraffin and sliced into 5 μ m sections. The sections were stained with hematoxylin and eosin (H&E) reagent. The whole pathological changes were observed at 100x and photographed under 200x by Leica Microsystems CMS GmbH Ernst-Leitz-Str.17-7 (Leica, Germany). A semi-quantitative histological score was used to assess the severity of ALI using a double-blind method. Histological indicators of lung injury included pulmonary edema, hemorrhage, alveolar wall thickening, alveolar structural destruction, leukocyte infiltration and interstitial hyperplasia. On a scale of 0–3, each item is divided into four levels (0, normal; 1, mild; 2, medium; 3, serious), calculating the total lung injury score [24].

2.7. Bronchoalveolar lavage fluid (BALF) collection

After euthanasia, the thorax and trachea of mice were exposed, the main trachea and the right pulmonary bronchus were ligated, and the left lung of the mice was irrigated with 0.4 mL pre-cooled PBS for three times. BALF was centrifuged at 350 g for 5 min at 4 °C. The supernatant was collected and stored in – 80 °C freezer until use. RBC was lysed with erythrocyte lysate and the cell pellet was resuspended in 200 μ L PBS and the total number of cells in BALF was calculated using TC20TM Automated Cell Counter (Bio-Rad Laboratories, Singapore).

2.8. Lung wet/dry weight ratio

The wet/dry (W/D) ratios were assessed reflecting the severity of

pulmonary edema. The middle lobe of the right lung was removed, rinsed briefly in saline and then weighed to obtain the wet weight. The lung was then dried at 60 °C in an oven to get the dry weight. The W/D ratios were calculated as dividing the wet weight by the dry weight.

2.9. Immunohistochemistry (IHC) and Immunofluorescence (IF) staining

For IHC analyses, paraffin-embedded sections were deparaffinized in xylene and rehydrated. After antigen retrieval with sodium citrate buffer, slides were treated with 3% H₂O₂ to quench endogenous peroxidase activity. Non-specific antibody binding was blocked by incubating slides with 10%FBS, after which slides were immunostained using the Neutrophil Elastase primary antibody (1:100; #ab68672), IL17A primary antibody (1:200; #ab79056) and PD-1 primary antibody (1:200; #18106-1-AP). Antibody-antigen complexes were detected using HRP-conjugated goat anti-rabbit secondary antibody (1:200, #ZB-2301) and visualized with a DAB substrate kit (#AR1022). The slides were then counterstained with Mayer's hematoxylin and differentiated with 1% hydrochloric acid alcohol. At the end, the slides were dehydrated and sealed. Stained slides were photographed and analyzed using Image J software. The positive area of at least 5 non-overlap fields was averaged for each stained slide.

For Immunofluorescence assay, slides were immunostained by using the F4/80 primary antibody (1:200; #ab6640). Antibody-antigen complexes were detected and visualized using Alexa Fluor®488-conjugated goat anti-Rat secondary antibody (1:200; Abcam, #150157). The nuclei were stained using Hoechst 33342, after that the slides were sealed.

2.10. Quantitative Real-Time polymerase chain reaction (qRT-PCR)

Total RNA samples from the lung tissues were extracted using TRIzol® reagent (Invitrogen, Thermo Fisher Scientific, Inc., Waltham, MA, USA) according to the manufacturer's protocol. RNA concentration was quantified by Nanodrop 2000. 2 μ g RNA samples were reverse transcribed into complementary DNA (cDNA) by Transcriptor First Strand cDNA Synthesis Kit (Roche, Mannheim, Germany). cDNA amplification was performed using the Bestar®Sybr Green qPCR Master Mix (DBI®-Bioscience, Ludwigshafen, Germany) in the Lightcycler480 II Real-Time PCR Detection System (Roche, Mannheim, Germany). GAPDH was used as an internal control. The comparative Ct method ($2^{-\Delta\Delta Ct}$) was used to analyze data. The sequences of primers for qRT-PCR are as Table 1.

2.11. Enzyme linked immunosorbent assay (ELISA)

The levels of TNF- α in serum were measured by the ELISA assay according to the manufacturer's instructions and the cytokine concentrations were calculated by using standard curves.

2.12. Data mining for network pharmacology

Except for gypsum, the active components and corresponding targets of the remaining 12 kinds of TCM included in the XFBD prescription were screened out from the Traditional Chinese Medicine Systems Pharmacology (TCMSP, <https://old.tcmsp-e.com/tcmsp.php>) database [25] and the Bioinformatics Analysis Tool for Molecular mechanism of Traditional Chinese Medicine (BATMAN, <http://bionet.ncpsb.org.cn/batman-tcm/>) database [26]. The targets of the compounds were supplemented through the PubMed database (<https://pubmed.ncbi.nlm.nih.gov/>). The targets for acute lung injury were obtained from the Gene Cards (<http://www.genecards.org/>) database [27] and the Comparative Toxicogenomic Database (CTD, <http://ctdbase.org/>) [28]. Protein-Protein Interaction (PPI) with high confidence (0.9) was analyzed in the STRING database (<https://www.string-db.org/>) [29]. The biological process (BP) enrichment analysis was conducted in the Database for Annotation, Visualization and Integrated Discovery (DAVID, <https://david.ncifcrf.gov/home.jsp>) [30]. We constructed the

Table 1
Primer sequences for RT-qPCR.

Primer name	Forward primer (5–3')	Reverse primer (5–3')
qMouse <i>Il1β</i>	GCAACTGTTCTGAACTCAACT	ATCTTTTGGGGTCCGTCAACT
qMouse <i>Il6</i>	TAGTCCTTCTACCCCAATTTCC	TTGGTCCTTAGCCACTCCTTC
qMouse <i>Tnf</i>	CCCTCACACTCAGATCATCTTCT	GCTACGACGTGGGCTACAG
qMouse <i>Il17a</i>	CTCAGACTACCTCAACCGTTCC	ATGTGGTGGTCCAGCTTTCC
qMouse <i>Pdcd1</i>	CATTCACTTGGGCTGTGCT	CAGGCTGGGTAGAAGGTGAG
qMouse <i>Muc5ac</i>	TACCACTCCCTGCTTCTGCAGCGTGCA	ATAGTAACAGTGGCCATCAAGGTCTGTCT
qMouse <i>Timp1</i>	GCAAAGAGCTTTCTCAAAGACC	AGGGATAGATAAACAGGGAAACACT
qMouse <i>Cxcl10</i>	CCAAGTGCTGCCGTCATTTTC	GGCTCGCAGGGATGATTTCAA
qMouse <i>Ccl2</i>	AAAACCTGGATCGGAACCAA	GCATTAGCTTCAGATTACGGGT
qMouse <i>Gapdh</i>	TGTGAAGCAGGCATCTGAG	TGCTGTGAAGTCGCAGGAG

network of TCM-compounds-targets-ALI and PPI by the Cystoscope software (version 3.2.1) [31]. Finally, we analyzed and established a target-pathway network associated with IL17A by Ingenuity Pathway Analysis.

2.13. Autodocking for virtual screening

The 3D structure of IL17A protein receptor was obtained from RCSB PDB database (<http://www.rcsb.org/>) under the PDB accession code 4hr9. The water molecules present in the crystal structure of IL17A was removed using Pymol-2.3.1 software, then Autodock tools-1.5.6 software was used to calculate the charge and add the atomic type, and then saved as pdbqt format file. PubChem database (<https://pubchem.ncbi.nlm.nih.gov/>) was used to download ligands. Autodock tools-1.5.6 software was used to calculate the atomic type and charge of ligands, which was also saved as pdbqt format file. Autodock Vina [32] was used to connect 10 active compounds (acteoside, amygdalin, ephedrine, hastatoside, glycyrrhizic acid, liquiritin, naringin, polydatin, sinapine and verbenaalin) as ligands with IL17A protein receptor. Subsequently, Pymol-2.3.1 was used to plot.

2.14. Biacore assay

The Biacore T200 and sensor chip CM5 are provided by Tianjin University of Science and Technology. The determination temperature was set at 25 °C. 1 × PBS buffer was used as the running buffer to activate the chip surface. The IL17A protein (#317-ILB-050) dissolved in 1 × PBS was added into 10 mM sodium acetate solution with pH 4.0 for protein conjugation. The 1.02 × PBS-P + buffer containing 2% DMSO was prepared as a small molecule sample running buffer. Solvent corrected fluids of 1.5% and 2.8% DMSO were formulated. Glycyrrhizic acid solution was diluted down by 2 times at 10 concentration gradients with 2% DMSO running buffer (1000 μM, 500 μM, 250 μM, 125 μM, 62.5 μM, 31.25 μM, 15.625 μM, 7.8125 μM, 3.90625 μM, 1.953125 μM). The protein binding time was 60 s and dissociation time was 120 s

2.15. Western Blot

Lung tissue lysate were collected with RIPA lysis containing 1% PMSF. Concentrations of protein were determined by the BCA Protein Assay Reagent Kit. 40 μg protein was separated by SDS-PAGE electrophoresis and transferred to PVDF Blotting Membrane (GE Healthcare Life science, Pittsburgh, US). After blocking with 5% fresh nonfat milk in tris-buffered saline containing 0.05% Tween-20, the membranes were incubated with IL17A primary antibody (1: 1000, #ab79056) overnight at 4 °C followed by HRP-conjugated goat anti-rabbit secondary antibody (1: 6000, #ZB-5301) incubation. GAPDH was used as an internal control. The probed bands were visualized by LI-COR Odyssey imaging system. The relative expression was quantified by Image J software.

2.16. IL17A blocking antibody experiments

Male C57BL/6 mice (20–23 g) were randomly divided into sham group (Sham), model group (LPS), XFBD high-dose treatment group (XFBD-H), IL17A blocking antibody group (IL17A mAb), XFBD high-dose and IL17A antibody combination group (XFBD-H +IL17A mAb), 5 in each group. 12 h after tracheal infusion of LPS, XFBD high dose was given once a day. Referring to the literature [33], IL-17A mAb (#16–7173–85) or IgG1K (#16–4714–85) was administered intravenously at a dose of 100 μg per mouse two days after treatment with LPS, to avoid blocking IL17A at the early stage of injury and affecting the recruitment of immune cells. All mice were euthanized 5 days later.

2.17. Statistical analysis

All quantitative data were shown as means ± SD and were performed with prism 6.0 (GraphPad, San Diego, CA, United States). Multi-group comparisons of the means were carried out by one-way analysis of variance (ANOVA) test with *post hoc* Tukey's test. $P < 0.05$ were considered as statistically significant.

3. Results

3.1. XFBD protects against LPS-induced ALI in vivo

In order to explore the efficacy of XFBD, we established ALI model by tracheal infusion of LPS and evaluated the disease status of mice on the 2nd day and 5th day after treatment of XFBD.

Fig. 1A demonstrated that XFBD treatment with different dosage could improve the weight loss of ALI mice from day 2. μ CT scanning results further showed that the diffuse infiltrating shadow and dense enhancement shadows (red arrow) appeared was effectively decreased after the 5 consecutive days-treatment of XFBD. While in the model group without any drug treatment, the shadow attenuation area of the lung field of mice increased on the 2nd day, indicating occurrence of pulmonary edema; The lung condition of mice subsequently deteriorated into pulmonary parenchymal lesions on the 5th day (Fig. 1B). We also used the WBP, a non-invasive animal lung function detection system to assess pulmonary function of LPS-induced ALI mice on the 2nd and 5th day. In contrast to saline-treated animals, the Penh (a surrogate measure of airway resistance/obstruction) of LPS-treated animals increased by 5.69 times (1.96 ± 0.82 vs 0.34 ± 0.03 , $P < 0.001$) on 2nd day (Fig. 1C), and the flow rate at 50% of the expired volume (EF50) increased by about 1.99 times (1.63 ± 0.51 vs 0.82 ± 0.12 , $P < 0.001$) at same time (Fig. 1D). After XFBD administered, it significantly improved the lung functions of ALI mice.

The lung wet/dry ratio and lung index were indicators to evaluate pulmonary edema. The wet/dry ratio of the right middle lobe of the lung of mice in the model group on the 2nd day and 5th day were about 1.70 times (5.97 ± 1.55 vs 3.57 ± 0.81 , $P < 0.01$) and 1.48 times (5.20 ± 0.17 vs 3.57 ± 0.81 , $P < 0.001$) respectively higher than that in the sham group, while the lung wet/dry ratio of XFBD-H group at 5th

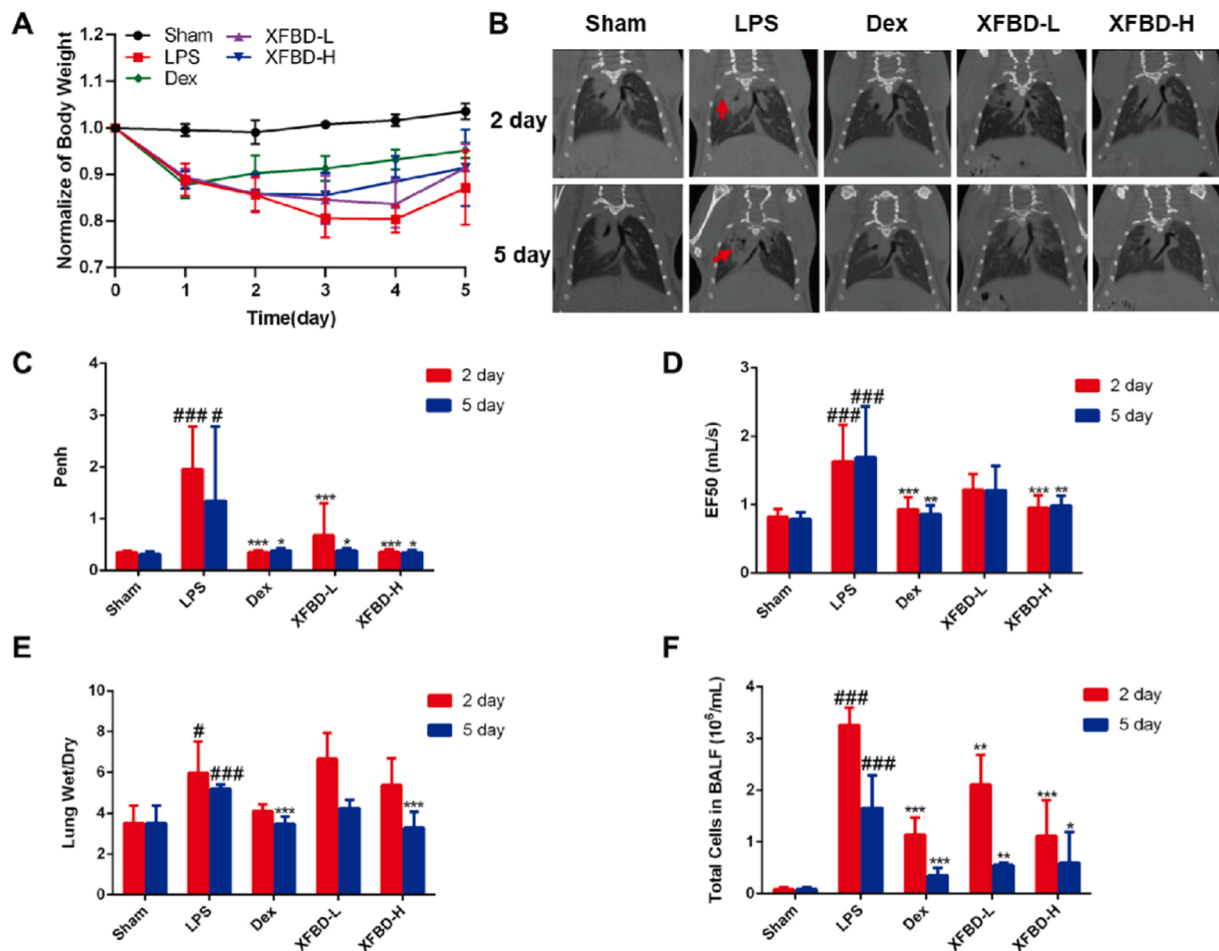


Fig. 1. XFBD protects against LPS-induced ALI. (A) Weight change curve of ALI mice. (B) μ CT scanning results of different stages of ALI mice. (C, D) Evaluation of Penh and EF50 of ALI mice on the 2nd and 5th day. (E) The wet/dry weight ratio of the right middle lobe of the lung of ALI mice on the 2nd and 5th day. Data were presented as mean \pm SD. # $P < 0.05$, ## $P < 0.01$, ### $P < 0.001$, vs. Sham group, * $P < 0.05$, ** $P < 0.01$, *** $P < 0.001$, vs. LPS group, $n = 6$.

day was down-regulated by 1.58 times (3.30 ± 0.71 vs 5.20 ± 0.17 , $P < 0.001$) (Fig. 1E). The lung index of mice in the model group on the 5th day increased by 1.86 times (0.01 ± 0.00 , $P < 0.001$) compared to sham group, which was reduced by XFBD effectively (Supplementary Fig. 1A). In addition, increased lung index and spleen index indicated immune dysfunction [34]. XFBD-H contributed to maintain immune function in ALI mice (Supplementary Fig. 1A and B). Moreover, we found that vastly increased inflammatory cells in the BALF after the treatment of LPS was significantly inhibited by XFBD-H on the 2nd day from 3.26 ± 0.34 to 1.12 ± 0.69 ($P < 0.001$) (Fig. 1F).

3.2. XFBD exerts protective effects on lung barrier and anti-inflammatory effects

To further elucidate the role of XFBD in mice treated with LPS, we evaluated the development of ALI by H&E staining. XFBD high dose had no toxic on the systematic organs (Supplementary Fig. 2). As shown in Fig. 2A, the results clearly showed atelectasis and collapse of alveoli, pulmonary edema (black arrow), and large amounts of red blood cell aggregation (yellow arrow) in the lung tissues of model group mice on the 2nd day after LPS induction, suggesting that the alveolar epithelium-vascular endothelial barrier was damaged. Alveolar structure damage and interstitial hyperplasia were more severe in the model group on the 5th day, and there was a persistent infiltration of inflammatory cells (blue arrow). After XFBD-H treatment for successive 5 days, the area of pulmonary edema, the levels of alveolar structure damage, interstitial

hyperplasia and inflammatory cells infiltration were significantly reduced (Fig. 2A and B).

Next, we detected the expression of pro-inflammatory cytokines including IL-6, TNF and IL-1 β . The expression of TNF- α in serum of the model group was still high on day 5, but it was not elevated under the protection of XFBD-H (Supplementary Fig. 3). Significantly, compared with the sham group, the expression of IL-6 mRNA in the lung tissue of the model group was increased by 3.60 times (3.61 ± 0.94 , $P < 0.001$), which was reduced to normal level by XFBD-H administration (Fig. 2C). The expression of *Tnf- α* mRNA in the lung tissue of the model group was increased by 3.27 times (3.41 ± 0.49 , $P < 0.001$) compared to sham group, XFBD treatment significantly inhibited its upregulation in a dose-dependent manner (Fig. 2D). The expression of IL-1 β mRNA in the lung tissue of the model group was increased by 3.94 times (4.19 ± 1.73 , $P < 0.05$); high dose administration of XFBD significantly inhibited the increase of IL-1 β mRNA in the lung tissue of mice (Fig. 2E). We also found that XFBD inhibit the expression of IL6, the activity of iNOS [35] and the expression of TNF- α in LPS-induced macrophages (Supplementary Fig. 4). Altogether, XFBD inhibited the expression and secretion of multi-cytokines, subsequently protected subunit-structures of pulmonary to against ALI development.

3.3. XFBD inhibits infiltration of macrophages and neutrophils in the LPS-induced ALI mice

We had found that XFBD could inhibit leukocyte infiltration. To

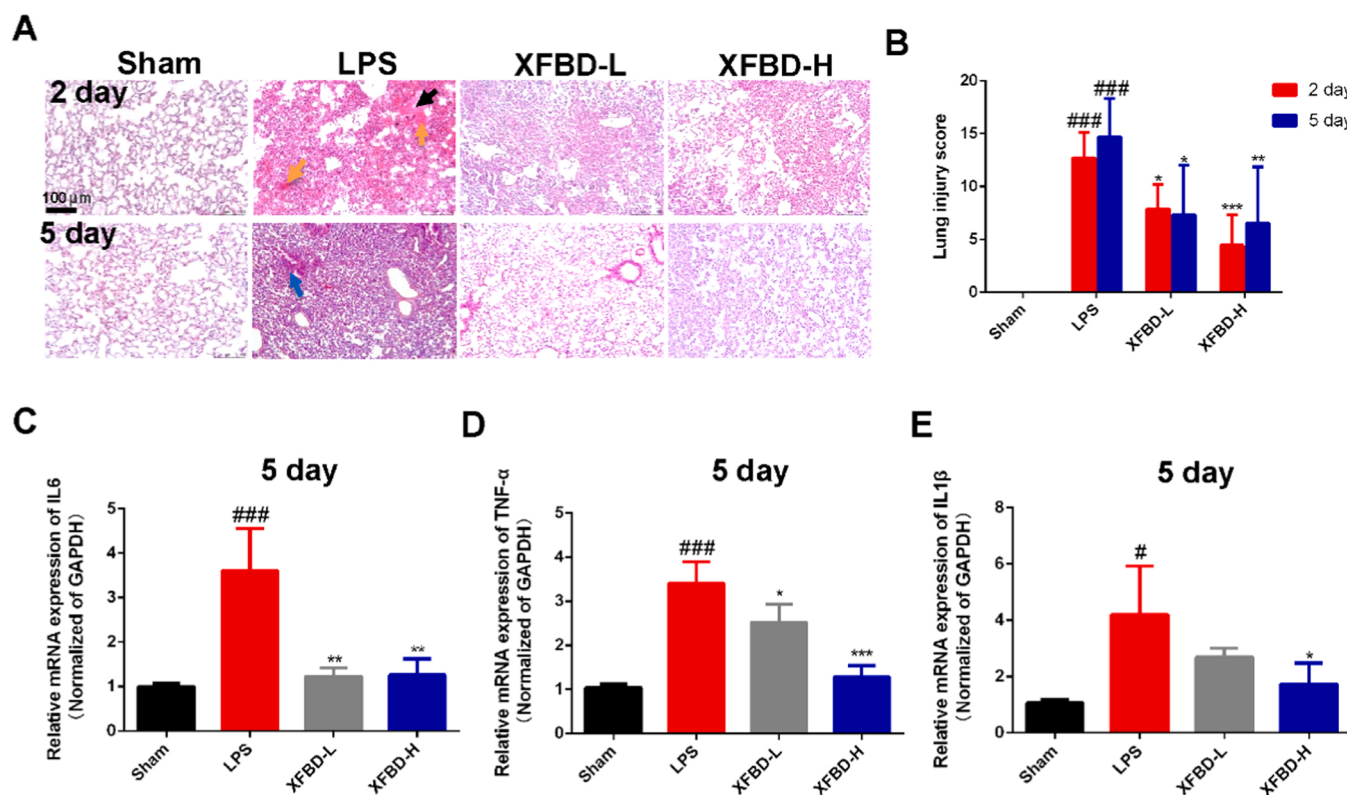


Fig. 2. XFBF exerts protective effects on lung barrier and anti-inflammatory effects in LPS-induced ALI mice. (A) Different stages of the histopathological of lung tissues after LPS treatment were evaluated by H&E staining, scale bar = 100 μ m. (B) Morphological damage score for the lung tissues, $n = 6$. The mRNA levels of *IL-6* (C), *Tnf- α* (D) and *IL-1 β* (E) in lung tissue on the 5th day, $n = 3$. Data were presented as mean \pm SD. ### $P < 0.01$, ### $P < 0.001$, vs. Sham group, * $P < 0.05$, ** $P < 0.01$, *** $P < 0.001$, vs. Model group.

explore whether neutrophils and macrophages are regulated by XFBF, we monitor the dynamics of immune cells in mice at different time points (0, 6, 12, 24, 48 h) after LPS infusion. As shown in Fig. 3A, the total white blood cell (WBC) count in peripheral blood (PB) of model group mice decreased sharply at 6 h, and gradually decreased with the extension of time, suggesting immune dysfunction in mice treated with LPS (Fig. 3A). To further investigate whether leukocytes were recruited from PB to the lung, we examined the total number of cells in BALF. The total number of cells in BALF increased at 6 h after LPS treatment, to the maximum value at 48 h and then decreased (Fig. 3B). In peripheral blood, the proportion of neutrophils in WBC increased first and then decreased, reaching the maximum value at 12 h; The proportion of lymphocytes decreased first and then increased, to the minimum value at 12 h; The proportion of monocytes increased first and then decreased, reaching the maximum value at 24 h; The ratios of eosinophils and basophils were almost unchanged (Fig. 3C). The result is consistent with the literature that neutrophils and monocytes/macrophages play an important role in ALI [7,8]. Therefore, neutrophils and macrophages as the main pathological cells in ALI were identified by neutrophil elastase (PMNE, which reflects neutrophils infiltration) immunohistochemistry staining and F4/80 immunofluorescence staining in lung tissue [36,37]. The increase of macrophages in the model group was reduced by 3.51 times (5.46 ± 0.82 vs 1.56 ± 0.61 , $P < 0.001$) by XFBF-H treatment on the 2nd day and 3.37 times (3.8 ± 0.74 vs 1.13 ± 0.75 , $P < 0.01$) on the 5th day (Fig. 3D and E). The increase of neutrophil elastase in the model group was reduced by 3.52 times (1.42 ± 0.40 vs 0.40 ± 0.12 , $P < 0.01$) after XFBF-H treatment on the 2nd day and 7.25 times (1.13 ± 0.39 vs 0.16 ± 0.07 , $P < 0.01$) on the 5th day (Fig. 3F and G). These results demonstrated that neutrophils and macrophages were recruited into the lungs in response to inflammatory signals, XFBF inhibited inflammatory response by inhibiting macrophages and neutrophils infiltration.

3.4. Analysis of candidate targets of XFBF against ALI

Based on the above experiments, we provide strong evidences for the role of XFBF in rescuing ALI. However, the pharmacodynamic basis and molecular mechanism of XFBF against ALI remain unclear. TCM prescriptions are characterized by multiple components, multiple targets and multiple pathways. Therefore, we synthesized anti-ALI components, targets and pathways in XFBF through network pharmacology.

Compounds with $OB \geq 30$ and $DL \geq 0.18$ were screened in TCMSP database, and compounds with $P < 0.05$ were screened in BATMAN-TCM database. A total of 329 compounds and 2109 targets contained in XFBF prescription were obtained after summarized. According to Relevance ≥ 50 in the GeneCards database and Score ≥ 50 in the CTD database, we obtained a total of 1172 ALI targets. There were 466 targets of XFBF against ALI (Fig. 4A). The network of TCM-compounds-targets-ALI was shown in Supplementary Fig. 5. 466 targets of XFBF against ALI are mainly involved in biological processes such as response to drug, apoptotic process, inflammatory response, etc. (Fig. 4B). The results of PPI showed that IL17A, STAT3, MAPK1, EP300, AKT1, CREBBP, JUN, PIK3CA and PIK3R1 may be major potential targets of XFBF in the treatment of ALI (Fig. 4C). We carried out the pathway enrichment analysis of the protein network with IL17A as the core, the result suggested that XFBF might play a protective role in LPS-induced ALI by targeting IL17A and regulating inflammatory signaling pathways such as IL17A, IL-6 and IL-8, as well as signaling pathways related to bacterial and viral infection and cell interaction (Fig. 4D).

To identify effective substances in XFBF that can regulate IL17A, we performed molecular docking with IL17A for the ten active ingredients in XFBF that had been detected by UHPLC [35]. The docking results are shown in Supplementary Table 1. The affinity less than -5.0 kJ/mol is taken as the screening standard, which indicates that it has decent binding activity. We found that the docking affinity of these active

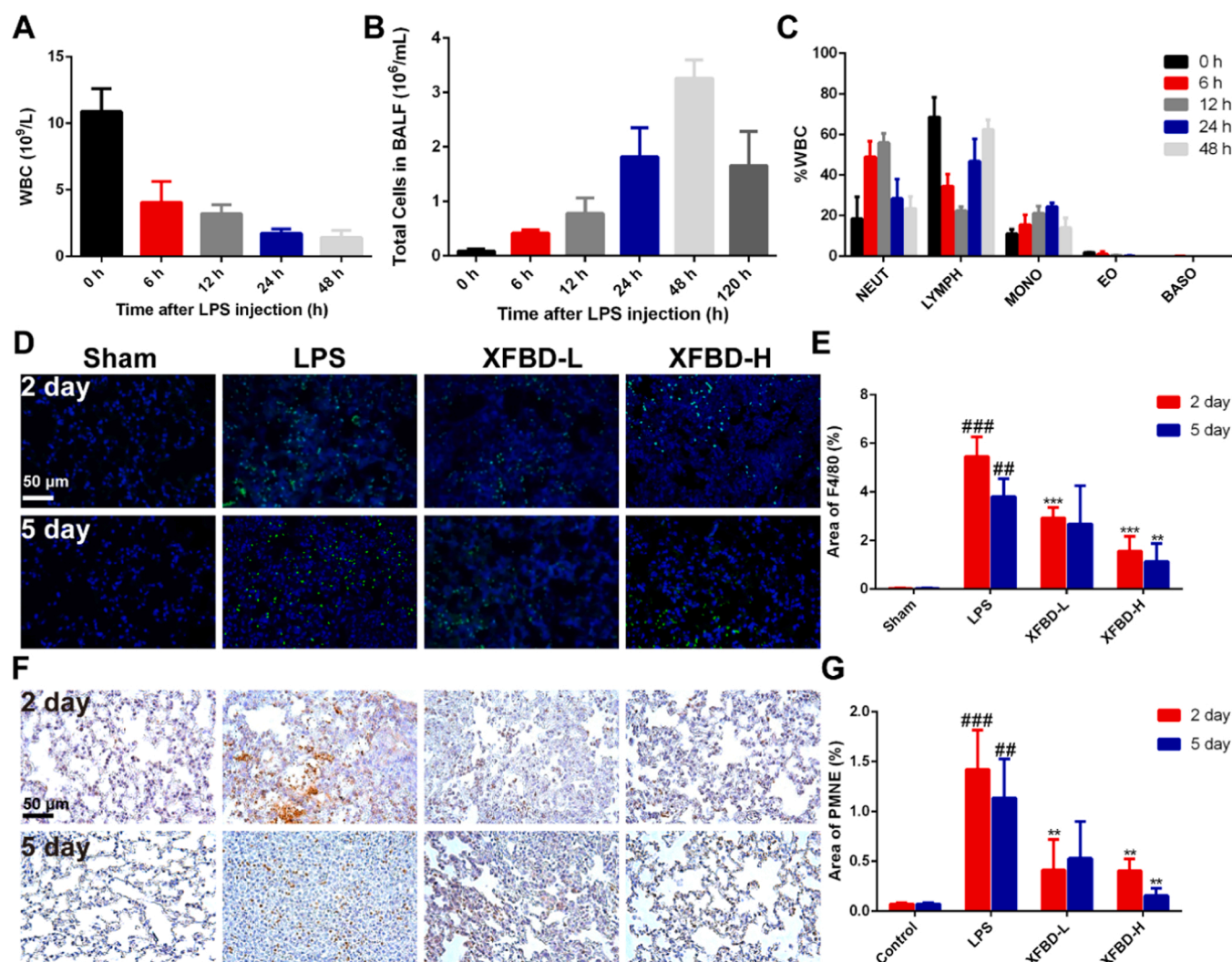


Fig. 3. XFBD inhibits infiltration of macrophages and neutrophils in the LPS-induced ALI mice. (A) The total number of white blood cells in PB at different time after LPS injection, $n = 5$. (B) The total cells count in BALF of ALI mice at different time after LPS injection. (C) The proportion of neutrophils, lymphocytes, monocytes, eosinophils and basophils in total leukocyte in PB at different time after LPS injection, $n = 5$. (D, E) Images and quantification of macrophages were identified by F4/80 Immunofluorescence staining in lung tissue, scale bar = 50 μm . (F, G) Images and quantification of neutrophils were identified by Immunohistochemistry staining of neutrophil elastase in lung tissue, scale bar = 50 μm . Data were presented as mean \pm SD. # $P < 0.05$, ## $P < 0.01$, ### $P < 0.001$, vs. Sham group, * $P < 0.05$, ** $P < 0.01$, *** $P < 0.001$, vs. Model group, $n = 3$.

compounds with IL17A were all less than -5.0 kJ/mol, indicating that the docking structures of these monomers with IL17A are relatively stable, and these compounds may be potential pharmacodynamic substances acting on IL17A against ALI. We selected four compounds with the lowest affinity (less than -8.0 kJ/mol) after docking with IL17A for further analysis. Based on the autodocking complex structures, the glycyrrhizic acid (GA) was stabilized by seven hydrogen bonds with IL17A residues TRP-67, LEU-97, ASP-45 and VAL-65 (Fig. 4E). The naringin was bound to IL17A through three hydrogen bonds with residues LYS-114, GLN-94 and TRP-91, as well as T-shaped π - π interaction with residue TYR-44 (Supplementary Fig. 6A). The acteoside was coordinated through seven hydrogen bonds with residues ASP-45, GLN-94, TYR-43, TYR-44 and GLU-95 (Supplementary Fig. 6B). The liquiritin interacts with IL17A through three hydrogen bonds with residues TRP-67, TYR-62 and LEU-97, π -cation interaction with residue LYS-114, and T-shaped π - π stacking interaction with residue TYR-62 (Supplementary Fig. 6C). We used the SPR-Biacore T200, a novel and straightforward methodology, to study protein–compound interactions. The result demonstrated that GA directly binds to IL17A in a concentration-dependent manner and has a micromolar binding affinity

($KD = 18.21$ μM) (Fig. 4F).

3.5. Transcriptome data revealed potential targets for XFBD reducing ALI

We performed transcriptome analysis on the lung tissues of mice in the sham group, LPS group and XFBD-H group for 5 days, to explore potential targets of XFBD in treatment for ALI. Compared with the sham group, the levels of 2949 genes were more than twice as significantly changed in the LPS group, and 1800 genes were regulated by XFBD-H (Fig. 5A). Clustering results of differentially expressed genes fully confirmed the effectiveness of XFBD in the treatment of ALI (Fig. 5B). Eliminating unknown genes, we further screened 265 key genes that had more than four-fold significant changes (Fig. 5C). Function & Disease enrichment analysis and pathway enrichment analysis of these key genes data were performed using IPA. They play an important role in gastrointestinal diseases, inflammatory diseases, inflammatory responses, organ damage, and cell migration, proliferation and transport (Fig. 5D), which may be closely related to the signaling pathway associated with IL17A, consistent with the results of systematic network pharmacology analysis (Fig. 5E). Through the IPA analysis, we deeply

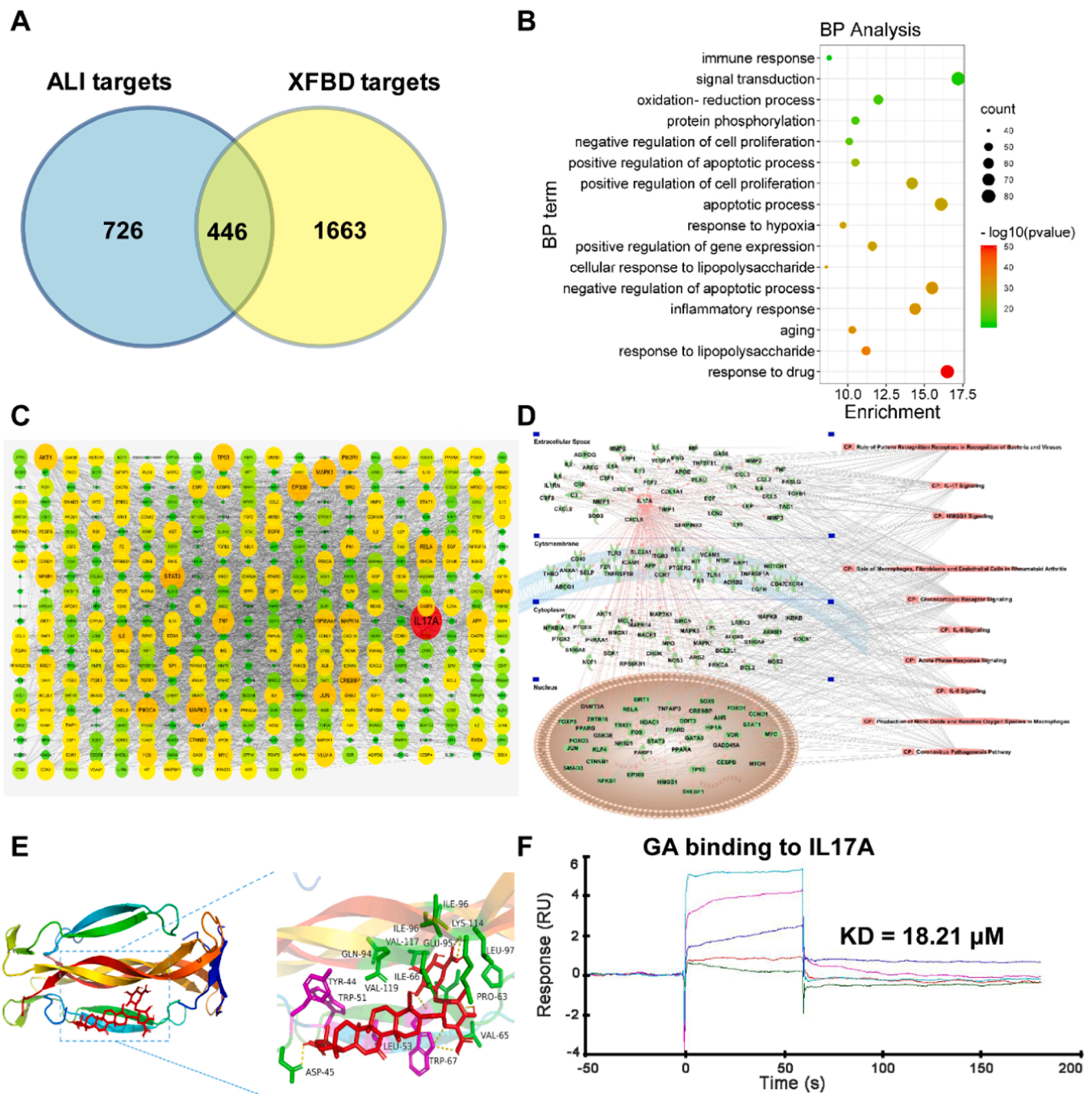


Fig. 4. Analysis of candidate targets of XFBD against ALI. (A) Venn Diagram revealed the overlapping genes between potential therapeutic targets of XFBD and lung injury targets. (B) Biological process analysis of overlapping genes. (C) PPI network of overlapping genes. (D) IL17A relative targets-pathway network. (E) Docking structure of glycyrrhizic acid with IL17A. (F) Biacore analysis of GA bonds to IL17A.

obtained the network with IL17A as the core in these 265 genes (Fig. 5F). The transcriptome data for the genes in the network were presented in Supplementary Table 2. Layer-by-layer analysis of the genomic data revealed that PD-1, IL17A and IL17A downstream targets including IL-6, CXCL10, CCL2, MPO, tissue inhibitor of metalloproteinases 1 (TIMP1) and mucin-5 subtype AC (MUC5AC) may be the potential anti-ALI targets of XFBD. They play a role in hyperinflammatory response, immune cells infiltration, vascular inflammation and airway damage, and collectively drive the disease toward pathology.

3.6. XFBD inhibited the overexpression of PD-1 and IL17A in the LPS-induced ALI mice

In order to determine whether the anti-ALI effect of XFBD was related to the IL17A/PD-1 pathway, we firstly detected the expression of IL17A and PD-1 in the lung tissues of ALI mice. We found that the protein expression of IL17A in lung tissues of mice in LPS group on the 5th day increased by about 1.92 times ($1.79 \pm 0.21, P < 0.01$) then that in sham group through Western Blot, which was reduced effectively by XFBD-H (Fig. 6A and B).

Additional results of Immunohistochemical staining and RT-qPCR also suggested that XFBD inhibited IL17A overproduction in lung

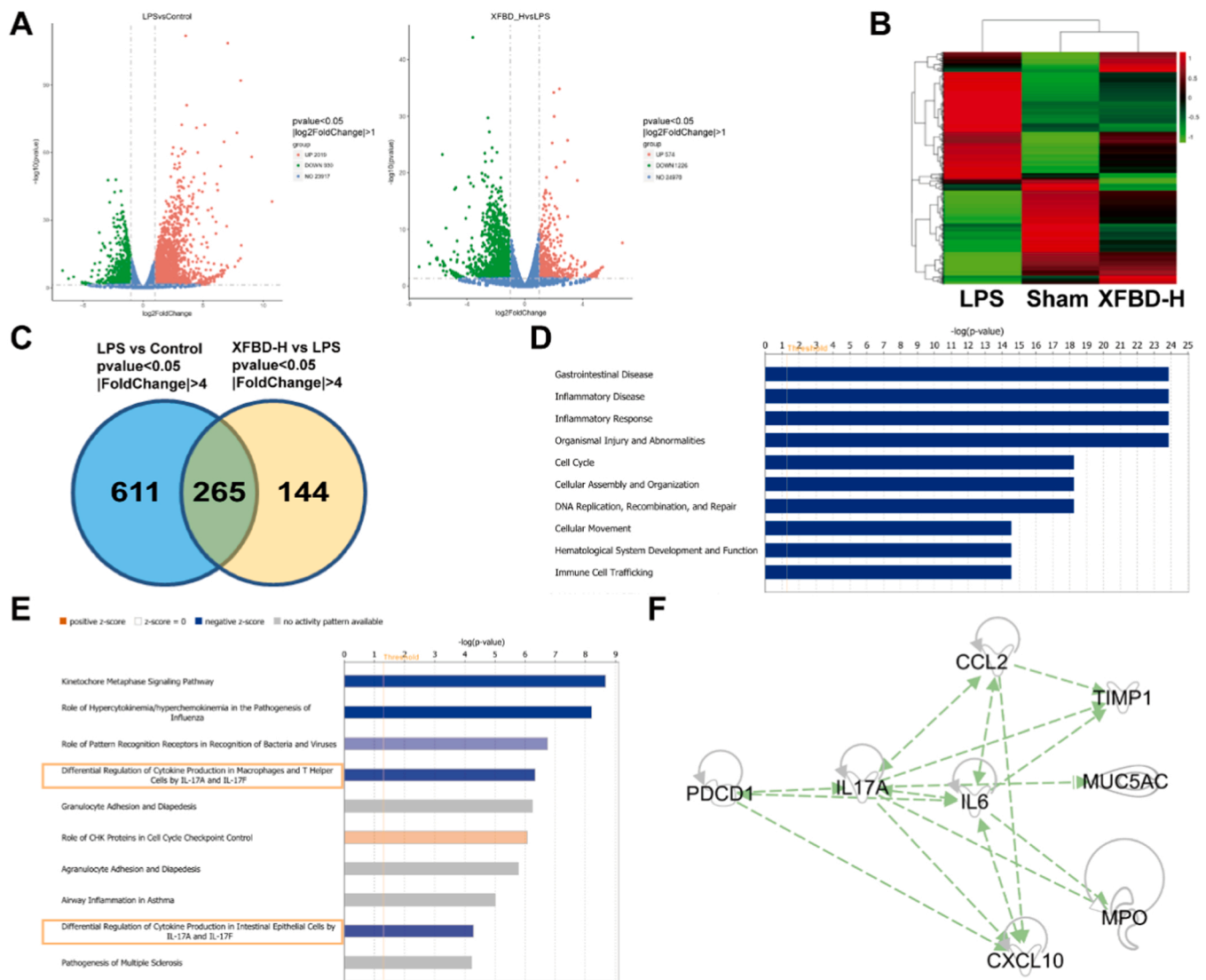


Fig. 5. Transcriptome data revealed potential targets for XFBD reducing ALI. (A) DEGs volcano map of LPS vs. Sham and XFBD-H vs. LPS. (B) DEGs volcano map of XFBD-H vs. LPS vs. Sham (C) DEGs Venn diagram with $P < 0.05$ and $|FC| > 4$. Different colors represent different combinations of comparisons. (D) Function & Disease enrichment analysis of 265 key genes by IPA. (E) Pathway enrichment analysis of 265 key genes by IPA. (F) Network relationship with IL17A as the core. The number of lung tissue samples tested was 3.

tissues (Fig. 6C–E). Conformably, we demonstrated that PD-1 was highly expressed in the lung tissues of ALI mice at both protein and transcriptional levels and significantly reduced in the XFBD-H group (Fig. 6F–H). Together, we identified the downstream targets of IL17A. As shown in Fig. 6I–L, XFBD inhibited LPS-induced upregulation of *Timp1*, *Muc5ac*, *Ccl2* and *Cxcl10* at high dose. The change in *Cxcl10* was particularly dramatic. The mRNA expression of *Cxcl10* in lung tissue of mice in model group was up to 31.69 times (33.93 ± 7.56 , $P < 0.001$) higher than that in sham group (Fig. 6L), this suggested that CXCL10 might play a powerful role in the exacerbation of ALI by PD-1/IL17A. And the MPO activity in lung tissue of mice in model group increased by 1.51 times (1.49 ± 0.08 , $P < 0.05$) compared to sham group, which was also decreased by XFBD-H significantly (Fig. 6M).

3.7. XFBD treated LPS-induced acute lung injury through PD-1/IL17A pathway

IL17A plays an important role in ALI, and our experiments proved that XFBD significantly inhibited the overexpression of PD-1, IL17A and downstream genes of IL17A. To further clarify whether XFBD can treat

LPS-induced acute lung injury through the PD-1/IL17A signaling pathway, as Fig. 7A showed, a high dose of XFBD was administrated 12 h after LPS treatment, and then IL17A mAb was used to block the IL17A pathway [33] at the early stage of injury on day 2. Firstly, μ CT results showed that the lung injury degree and shadow area of mice in the XFBD-H treatment group, IL17A mAb group and XFBD-H+IL17A mAb group were all reduced (Fig. 7B). The inhibitory effect of XFBD-H on increased spleen index was comparable to that of IL17A mAb (Fig. 7C). The ratio of lung wet-dry in mice treated with XFBD-H and mice treated with IL17A mAb was 1.28 times (4.15 ± 0.25) and 1.51 times (3.52 ± 0.18) lower than that in the model group, respectively (Fig. 7D). After treatment of XFBD-H or IL17A mAb, total number of cells in BALF was decreased (Fig. 7E). Next, we examined the expression of inflammatory cytokines including IL-6 and TNF- α in lung tissue. Both XFBD-H and IL17A mAb could decrease the transcription level of *Tnf- α* and *Il-6* (Fig. 7F and Supplementary Fig. 7).

We performed qualitative and quantitative analysis of macrophages and neutrophils in lung tissues. As shown in Fig. 8A–D, the infiltration of macrophages and neutrophils in the lung tissues of ALI mice was significantly reduced after treatment with XFBD-H and IL17A mAb.

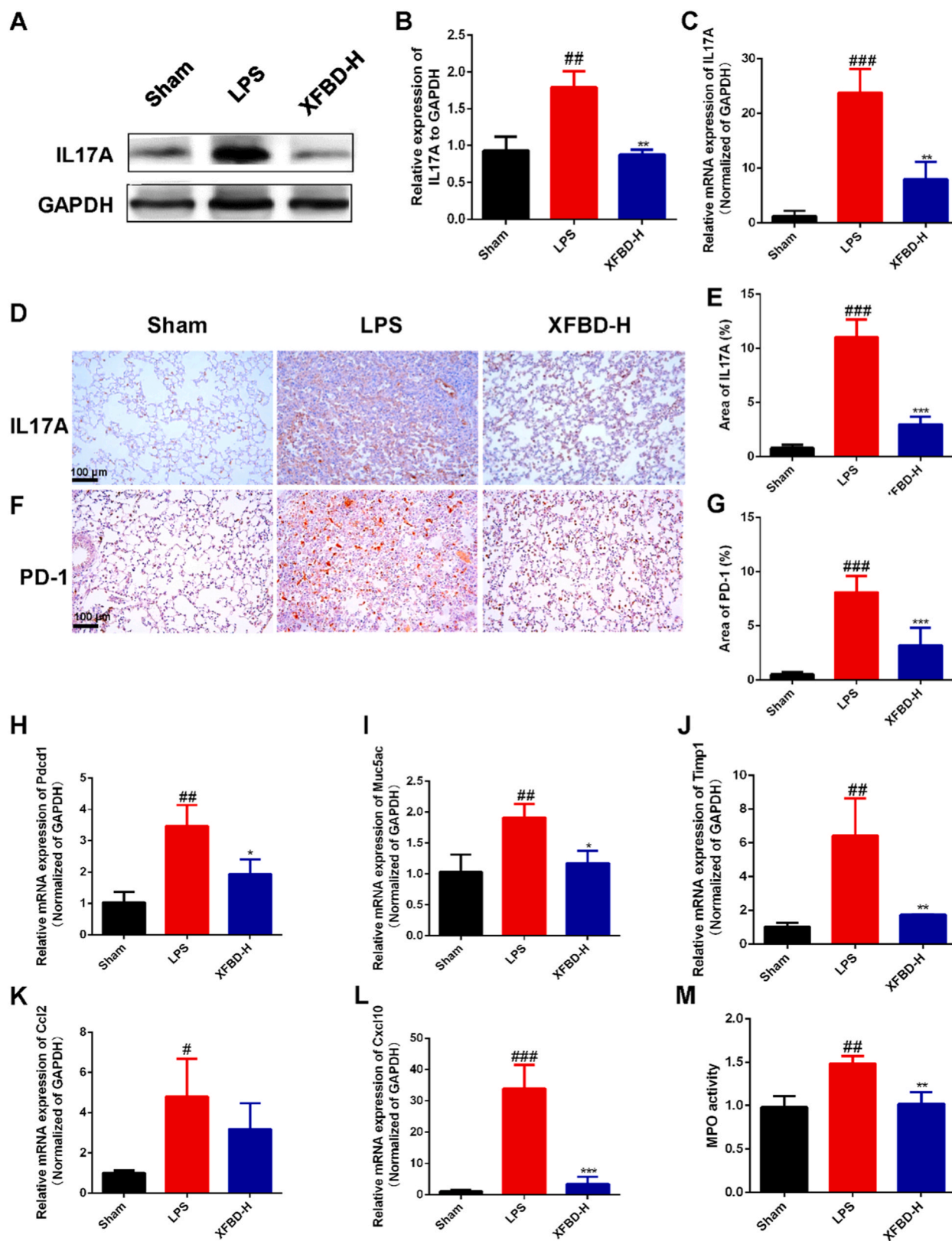


Fig. 6. XFBD inhibited the overexpression of PD-1 and IL17A in the LPS-induced ALI mice. (A, B) The IL17A in lung tissues of mice after 5 days of LPS infusion were measured by Western Blot. (C) The mRNA levels of *Il17a* in lung tissues of mice after 5 days of LPS infusion. (D-G) The IL17A and PD-1 in lung tissues of mice after 5 days of LPS infusion was measured by Immunohistochemical staining. The mRNA levels of *Pcdcl1* (H), *Muc5ac* (I), *Timp1* (J), *Ccl2* (K), *Cxcl10* (L). (M) The MPO activity in lung tissues of mice after 5 days of LPS infusion. Data were presented as mean \pm SD. * $P < 0.05$, ** $P < 0.01$, *** $P < 0.001$, vs. Sham group, * $P < 0.05$, ** $P < 0.01$, *** $P < 0.001$, vs. Model group, $n = 3$.

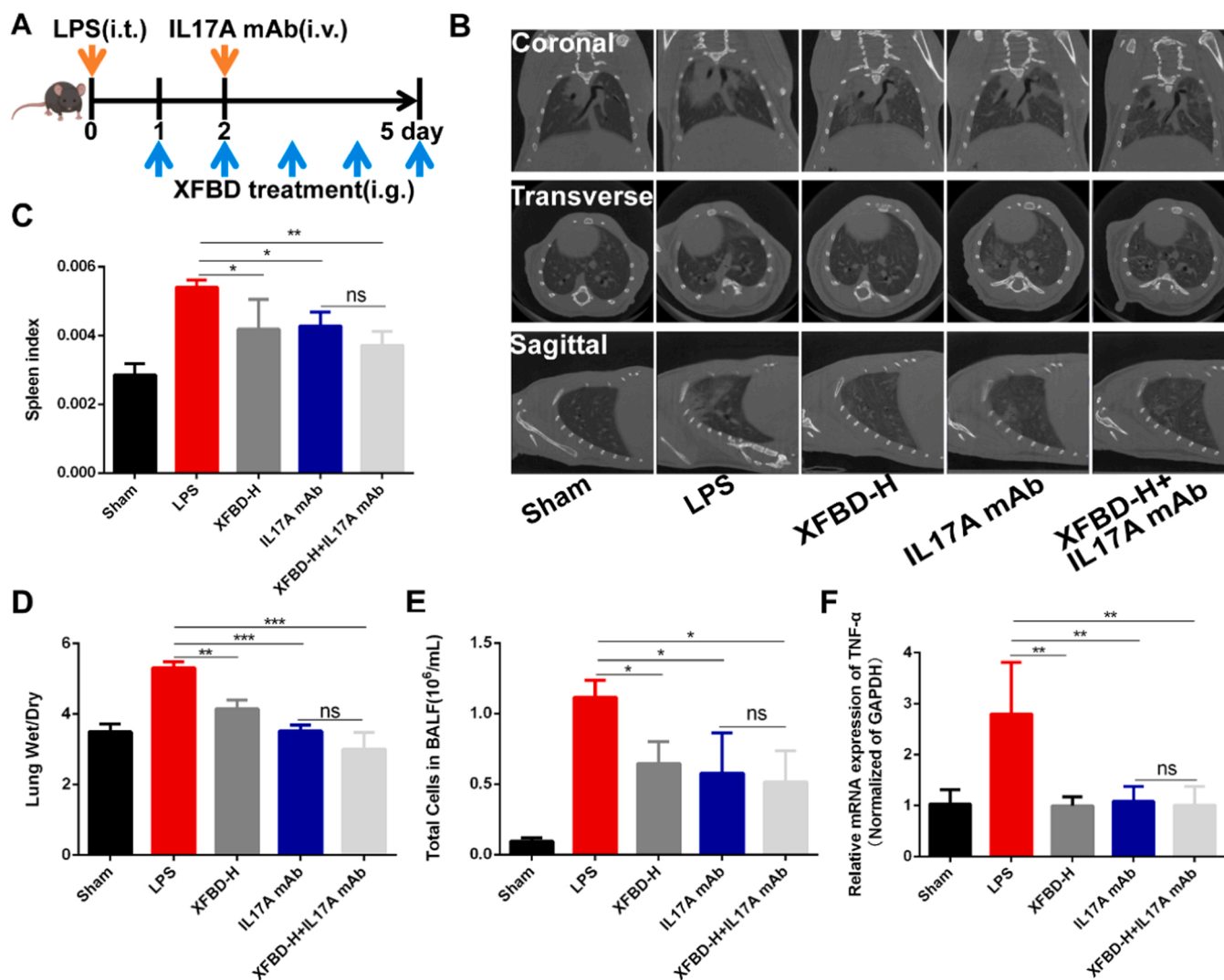


Fig. 7. XFBH treated LPS-induced acute lung injury (A) The scheme of IL17A blocking antibody experiment. (B) μ CT scanning results. (C) Spleen index of ALI mice after XFBH-H or IL17A mAb treatment. (D) The ratio of lung wet-dry. (E) Total cells in BALF of ALI mice after XFBH-H or IL17A mAb treatment. (F) The gene expression of *Tnf- α* in lung tissues of ALI mice after XFBH-H or IL17A mAb treatment, $n = 3$. Data were presented as mean \pm SD. * $P < 0.05$, ** $P < 0.01$, *** $P < 0.001$, vs. Model group.

Finally, we validated genes in the IL17A signaling pathway. The results showed that XFBH-H could significantly reduce the transcription levels of *Il17a* and *Pdcd1*, which was superior to IL17A mAb (Fig. 8E and F). In addition, XFBH-H also significantly inhibited the overexpression of downstream targets of IL17A, including *Ccl2*, *Cxcl10* and *Timp1*, especially for *Cxcl10*, which was comparable to effects of XFBH in preventing ALI (Fig. 8G, H and Supplementary Fig. 8). IL17A mAb showed better efficacy, however, all these results showed that there was no statistical difference between the XFBH-H+IL17A mAb group and the IL17A mAb group, indicating that XFBH treated LPS-induced ALI mainly through PD-1/IL17A signaling pathway.

4. Discussion and conclusion

COVID-19 is polyphasic in nature, with secondary cytokine storm and ARDS resulting in poor outcomes, plus overwhelmed intensive care units and hospitals [38]. At the beginning of the COVID-19 outbreak, a number of antiviral medicines have been used to reduce the viral load. However, in clinical practice, patients are unlikely to be detected early enough (i.e., before/at symptom onset) to benefit from antiviral strategies. Inhibiting excessive inflammation response may be more promising strategy to prevent COVID-19 from turning into severe disease.

Tocilizumab (IL6/IL6R inhibitor) [39], adalimumab (TNF inhibitor) [40], secukinumab (IL-17 inhibitor), brodalumab (IL17R inhibitor) [15], etc. already had been proposed to regulate the cytokine release syndrome during the development of COVID-19. Additionally, the vaccines against COVID-19 have benefited the whole country, and has been included in the list of emergency use by WHO.

Xuanfei Baidu Decoction for the treatment of COVID-19 patients with dampness-toxic and lung-stagnation syndrome has shown unique advantages in reducing the transformation of mild patients to severe diseases [19]. However, basic research on XFBH is lacking, and its mechanism is unclear. Mouse models of direct ALI were established by intratracheal or intranasal administration of lipopolysaccharide, hydrochloric acid, live (or heat-killed) bacteria and viruses; Intravenous LPS, cecal ligation and puncture, hemorrhagic shock and mesenteric ischemia-reperfusion cause indirect lung injury [41]. LPS from *E. coli* is used to simulate bacterial infection and as an activator of innate immunity [42]. LPS-induced ALI is a well-characterized, repeatable and highly similar ALI model [43]. In our study, intratracheal LPS infusion did cause severe pulmonary edema, diffuse alveolar injury, leukocyte infiltration and inflammatory cytokine secretion.

We demonstrated that XFBH could resist the progression of LPS-induced ALI. XFBH improved lung function, reduced pulmonary

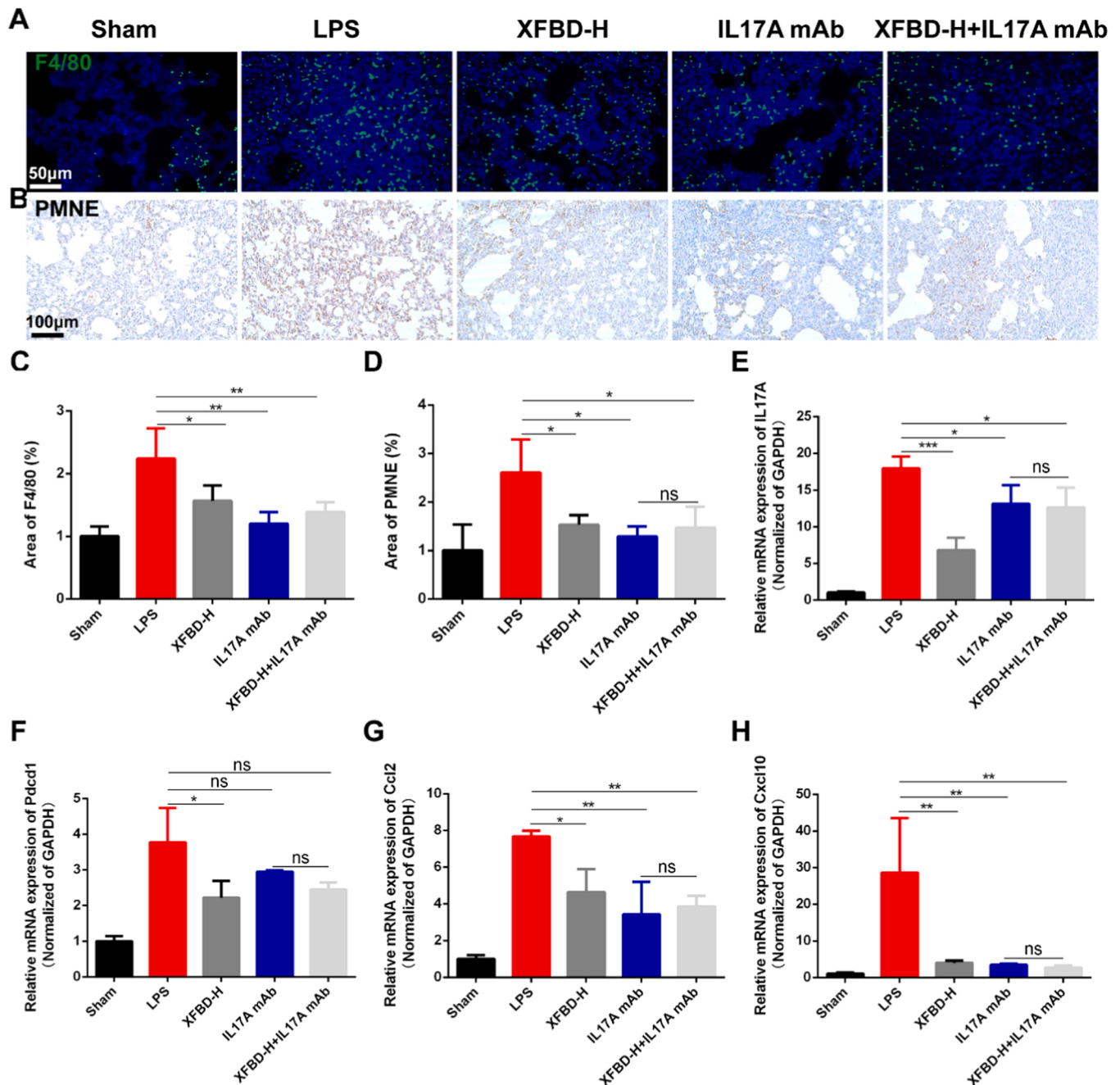


Fig. 8. XFBF treated LPS-induced acute lung injury through PD-1/IL17A pathway (A, C) The changes of macrophages in IL17A blocking antibody experiment. (B, D) The changes of neutrophils in IL17A blocking antibody. (E-H) The gene expression of *Il17a*, *Pdcd1*, *Ccl2* and *Cxcl10* in lung tissues of ALI mice after XFBF-H or IL17A mAb treatment, $n = 3$. Data were presented as mean \pm SD. * $P < 0.05$, ** $P < 0.01$, *** $P < 0.001$, vs. Model group.

edema, inhibited inflammatory cells infiltration and the over-expression of inflammatory cytokine, and protect lung tissue against destruction. Specifically, we found that XFBF could modulate the recruitment of macrophages and neutrophils, thereby achieving significant anti-inflammatory effect. The results of network pharmacology and transcriptomics revealed that IL17A may be the main target of XFBF against ALI. Consistent with the analysis, we verified that XFBF inhibited the expression of multiple genes, including *Pdcd1*, *Il17a*, *Ccl2*, *Cxcl10*, *Mpo*, *Timp1* and *Muc5ac*. Further, we performed IL17A blocking antibody experiments to elucidate the immunomodulatory mechanism of XFBF which is mainly focused on the PD-1/IL17A axis to regulate neutrophils and macrophages infiltration, thereby retarded the development of ALI. We attempted to provide some material basis to support the

pharmacological effects of XFBF. Through molecular docking and Biacore experiment, we revealed that glycyrrhizic acid, etc. can effectively bind to IL17A. In fact, many of the compounds contained in XFBF have been reported their anti-inflammatory and immunomodulatory effects. For example, GA inhibited neutrophils accumulation in BALF of murine chronic obstructive pulmonary disease (COPD) model possibly due to the blocking of IL17A signaling pathway [44]; While Polydatin inhibited the expression of NF- κ B in LPS-induced ALI model, which could reduce IL17A secretion [45,46]. These may cause a synergistic effect between compounds that act indirectly on IL17A and bind directly to IL17A.

The effects of IL17A are tremendous. The signature function of IL17A is that it acts on various of adjacent cells driving the production of inflammatory cytokines and chemokines such as IL-6, CCL2 and CXCL10,

which recruit bone-marrow derived cells, such as neutrophils and macrophages, into infected tissues [47,48]. As is known to all, IL-6 was a devastating force in the inflammatory storm of many immune diseases. In addition, transcriptome sequencing of RNA isolated from BALF and peripheral blood mononuclear cells (PBMC) samples from COVID-19 patients revealed an association between COVID-19 pathogenesis and excessive release of CCL2 and CXCL10 [49]. CCL2 mainly recruits monocyte/macrophages through the CCL2-CCR2 axis [50]. Single-cell transcriptome analysis highlighted the role of neutrophils and inflammatory macrophages in the pathogenesis of severe COVID-19, with CCL2 associated with macrophage cluster-1 in patients with severe COVID-19 [51]. IL17A could cooperate with CCL2 to promote specific overexpression of TIMP1 in mouse pneumonia lesions [52]. Its levels are higher in patients with ARDS and are associated with more severe hypoxemia and poorer prognosis [53]. It was worth mentioning that increased CXCL10 level was largely from lung neutrophils in the lungs of non-viral and viral ARDS mice, CXCL10 acted in an autocrine manner on the oxidative rupture and chemotaxis of inflammatory neutrophils, leading to fulminant pulmonary inflammation [3].

There is little literature suggesting that IL17A might be regulated by programmed death 1 protein (PD-1). PD-1 encoded by the *Pdcd1* gene is a co-suppressor protein on the surface of immune cells including neutrophils and macrophages that plays a role in autoimmune diseases, tumor cell survival and viral infections [54]. The strategy of blocking PD-1/PD-L1 is widely applicable to clinical cancer treatment. However, there are few studies on PD-1 in ALI. Sean F. M. et al. exploited novel role of PD-1 in a murine model of indirect-acute lung injury by cecal ligation & puncture-septic challenge, which was associated with increased number of PD-1 positive immunocell in the lungs [54]. Lindsay J Celada, et al. found that PD-1 blockade reduced STAT3-mediated IL17A production in CD4⁺T cell to treat pulmonary fibrosis [55]. The role of PD-1/IL17A in LPS-induced ALI and its communication with other immune cells such as macrophages and neutrophils remain to be explored. Innovatively, we elucidated the novel role of PD-1, which acts on IL17A and promotes the recruitment of macrophages and neutrophils, leading to ALI.

In conclusion, vaccination against COVID-19 is an inevitable trend, but identifying effective treatments remains a crucial task. Here, we explored the pharmacodynamics of XFBD in LPS-induced ALI based on clinical application. Combining systematic pharmacological and transcriptome studies, we revealed mechanisms by which XFBD improved ALI. We concluded that XFBD could treat ALI by inhibiting the PD-1/IL17A signaling pathway to balance immune cell homeostasis and reduce hyperinflammatory response. This provides insight into the clinical treatment of COVID-19 with XFBD.

CRediT authorship contribution statement

J.Y. and H.Z. designed the experiments. Y.Y.W. performed the biological experiments of acute lung injury model and X.W performed the protein auto-docking analysis. X.W., Y.X.L. and Z.F.X. assisted the study. Y.Y.W., X.W., R.S. and Z.F.X., drafted the manuscript. All authors read and approved the final manuscript.

Declaration of Competing Interest

The authors declare that they have no known competing financial interests or personal relationships that could have appeared to influence the work reported in this paper.

Acknowledgements

This work was supported by National Key R&D Program of China [2020YFA0708004]; and the grant from National Natural Science Foundation of China [No. 82074032].

Appendix A. Supporting information

Supplementary data associated with this article can be found in the online version at [doi:10.1016/j.phrs.2022.106083](https://doi.org/10.1016/j.phrs.2022.106083).

References

- [1] A.F. Rendeiro, H. Ravichandran, Y. Bram, V. Chandar, J. Kim, C. Meydan, J. Park, J. Foox, T. Hether, S. Warren, Y. Kim, J. Reeves, S. Salvatore, C.E. Mason, E. C. Swanson, A.C. Borczuk, O. Elemento, R.E. Schwartz, The spatial landscape of lung pathology during COVID-19 progression, *Nature* 593 (2021) 564–569, <https://doi.org/10.1038/s41586-021-03475-6>.
- [2] M.Z. Tay, C.M. Poh, L. Rénia, P.A. MacAry, L.F.P. Ng, The trinity of COVID-19: immunity, inflammation and intervention, *Nat. Rev. Immunol.* 20 (2020) 363–374, <https://doi.org/10.1038/s41577-020-0311-8>.
- [3] A. Ichikawa, K. Kuba, M. Morita, S. Chida, H. Tezuka, H. Hara, T. Sasaki, T. Ohteki, V.M. Ranieri, C.C. dos Santos, Y. Kawaoka, S. Akira, A.D. Luster, B. Lu, J. M. Penninger, S. Uhlig, A.S. Slutsky, Y. Imai, CXCL10-CXCR3 enhances the development of neutrophil-mediated fulminant lung injury of viral and nonviral origin, *Am. J. Respir. Crit. Care Med.* 187 (2013) 65–77, <https://doi.org/10.1164/rccm.201203-0508OC>.
- [4] J.N. Gustine, D. Jones, Immunopathology of hyperinflammation in COVID-19, *Am. J. Pathol.* 191 (2021) 4–17, <https://doi.org/10.1016/j.ajpath.2020.08.009>.
- [5] E.T. Obadina, J.M. Torrealba, J.P. Kanne, Acute pulmonary injury: high-resolution CT and histopathological spectrum, *Br. J. Radiol.* 86 (2013), 20120614, <https://doi.org/10.1259/bjr.20120614>.
- [6] A. Synowiec, A. Szczepański, E. Barreto-Duran, L.K. Lie, K. Pyrc, Severe acute respiratory syndrome coronavirus 2 (SARS-CoV-2): a systemic infection, *Clin. Microbiol. Rev.* 34 (2021), <https://doi.org/10.1128/cmr.00133-20>.
- [7] J. Lei, Y. Wei, P. Song, Y. Li, T. Zhang, Q. Feng, G. Xu, Cordycepin inhibits LPS-induced acute lung injury by inhibiting inflammation and oxidative stress, *Eur. J. Pharmacol.* 818 (2018) 110–114, <https://doi.org/10.1016/j.ejphar.2017.10.029>.
- [8] J. Zhao, H. Yu, Y. Liu, S.A. Gibson, Z. Yan, X. Xu, A. Gaggar, P.K. Li, C. Li, S. Wei, E. N. Benveniste, H. Qin, Protective effect of suppressing STAT3 activity in LPS-induced acute lung injury, *Am. J. Physiol. Lung Cell Mol. Physiol.* 311 (2016) L868–L880, <https://doi.org/10.1152/ajplung.00281.2016>.
- [9] R. Ye, Z. Liu, ACE2 exhibits protective effects against LPS-induced acute lung injury in mice by inhibiting the LPS-TLR4 pathway, *Exp. Mol. Pathol.* 113 (2020), 104350, <https://doi.org/10.1016/j.yexmp.2019.104350>.
- [10] H. Oh, S.H. Park, M.K. Kang, Y.H. Kim, E.J. Lee, D.Y. Kim, S.I. Kim, S. Oh, S.S. Lim, Y.H. Kang, Asaronic acid attenuates macrophage activation toward M1 phenotype through inhibition of NF- κ B pathway and JAK-STAT signaling in glucose-loaded murine macrophages, *J. Agric. Food Chem.* 67 (2019) 10069–10078, <https://doi.org/10.1021/acs.jafc.9b03926>.
- [11] S.E. Park, K. Sapkota, S. Kim, H. Kim, S.J. Kim, Kaempferol acts through mitogen-activated protein kinases and protein kinase B/AKT to elicit protection in a model of neuroinflammation in BV2 microglial cells, *Br. J. Pharmacol.* 164 (2011) 1008–1025, <https://doi.org/10.1111/j.1476-5381.2011.01389.x>.
- [12] N. Somensi, T.K. Rabelo, A.G. Guimarães, L.J. Quintans-Junior, A.A. de Souza Araújo, J.C.F. Moreira, D.P. Gelain, Carvacrol suppresses LPS-induced pro-inflammatory activation in RAW 264.7 macrophages through ERK1/2 and NF- κ B pathway, *Int. Immunopharmacol.* 75 (2019), 105743, <https://doi.org/10.1016/j.intimp.2019.105743>.
- [13] J.G. Park, Y.J. Son, B.C. Yoo, W.S. Yang, J.H. Kim, J.H. Kim, J.Y. Cho, Syk plays a critical role in the expression and activation of IRAK1 in LPS-treated macrophages, *Mediat. Inflamm.* 2017 (2017), 1506248, <https://doi.org/10.1155/2017/1506248>.
- [14] M. Ju, B. Liu, H. He, Z. Gu, Y. Liu, Y. Su, D. Zhu, J. Cang, Z. Luo, MicroRNA-27a alleviates LPS-induced acute lung injury in mice via inhibiting inflammation and apoptosis through modulating TLR4/MyD88/NF- κ B pathway, *Cell Cycle* 17 (2018) 2001–2018, <https://doi.org/10.1080/15384101.2018.1509635>.
- [15] O. Pacha, M.A. Sallman, S.E. Evans, COVID-19: a case for inhibiting IL-17? *Nat. Rev. Immunol.* 20 (2020) 345–346, <https://doi.org/10.1038/s41577-020-0328-z>.
- [16] M. Wu, T. Lai, D. Jing, S. Yang, Y. Wu, Z. Li, Y. Wu, Y. Zhao, L. Zhou, H. Chen, J. Shen, W. Li, S. Ying, Z. Chen, X. Wu, H. Shen, Epithelium-derived IL17A Promotes Cigarette Smoke-induced Inflammation and Mucus Hyperproduction, *Am. J. Respir. Cell Mol. Biol.* DOI 10.1165/rcmb.2020-0424OC(2021). <https://doi.org/10.1165/rcmb.2020-0424OC>.
- [17] M. Tang, L. Lu, X. Yu, Interleukin-17A interweaves the skeletal and immune systems, *Front. Immunol.* 11 (2020), 625034, <https://doi.org/10.3389/fimmu.2020.625034>.
- [18] V. Bulat, M. Situm, M.D. Azdajic, R. Likić, Potential role of IL-17 blocking agents in the treatment of severe COVID-19? *Br. J. Clin. Pharmacol.* 87 (2021) 1578–1581, <https://doi.org/10.1111/bcp.14437>.
- [19] H. Wang, H.X. Song, D.F. Wang, X.R. Ma, D.X. Zou, J.X. Miao, Y.L. Wang, W. P. Yang, The molecular mechanism of Xuanfei Baidu Formula in the treatment of COVID-19 antiviral effect based on network pharmacology and molecular docking, *J. Hainan Med. Univ.* 26 (2020) 1361–1372, <https://doi.org/10.13210/j.cnki.jhmu.20200617.003>.
- [20] L. Zhou, X. Wang, X. Liu, X. Fei, L. Liu, Z. Liu, K. Wang, W. Zhang, S. Qiao, X. Li, W. Pang, Q. Liu, Case report of Xuanfei Baidu Decoction for curing severe cases of COVID-19, *Tianjin, J. Tradit. Chin. Med.* 38 (2021) 556–559, <https://doi.org/10.11656/j.issn.1672-1519.2021.05.03>.

- [21] Y. Wang, X. Li, H. Zang, J.H. Zang, R. Xue, J.Y. Qian, Q.Q. Liu, X.H. Fan, Y. Cheng, X.H. Zhang, B.L. Zhang, Mechanism of Xuanfei Baidu Tang in treatment of COVID-19 based on network pharmacology, China, J. Chin. Mater. Med. 45 (2020) 2249–2256, <https://doi.org/10.19540/j.cnki.cjmm.20200325.401>.
- [22] S. Li, M. Zang, P. Wang, F. Hong, C. Wang, Y. Zhang, Z. Geng, X. Yang, X. He, Y. Sun, F. Yang, The significance of a non-invasive measurement of lung function in mice, Acta Lab Anim. Sci. Sin. 26 (2018) 549–553, <https://doi.org/10.3969/j.issn.1005-4847.2018.05.002>.
- [23] T.P. Sheahan, A.C. Sims, S.R. Leist, A. Schafer, J. Won, A.J. Brown, S. A. Montgomery, A. Hogg, D. Babusis, M.O. Clarke, J.E. Spahn, L. Bauer, S. Sellers, D. Porter, J.Y. Feng, T. Cihlar, R. Jordan, M.R. Denison, R.S. Baric, Comparative therapeutic efficacy of remdesivir and combination lopinavir, ritonavir, and interferon beta against MERS-CoV, Nat. Commun. 11 (2020) 222, <https://doi.org/10.1038/s41467-019-13940-6>.
- [24] C. Song, H. Li, Y. Li, M. Dai, L. Zhang, S. Liu, H. Tan, P. Deng, J. Liu, Z. Mao, Q. Li, X. Su, Y. Long, F. Lin, Y. Zeng, Y. Fan, B. Luo, C. Hu, P. Pan, NETs promote ALL/ARDS inflammation by regulating alveolar macrophage polarization, Exp. Cell Res. 382 (2019), 111486, <https://doi.org/10.1016/j.yexcr.2019.06.031>.
- [25] J. Ru, P. Li, J. Wang, W. Zhou, B. Li, C. Huang, P. Li, Z. Guo, W. Tao, Y. Yang, X. Xu, Y. Li, Y. Wang, L. Yang, TCMSP: a database of systems pharmacology for drug discovery from herbal medicines, J. Cheminform. 6 (2014) 13, <https://doi.org/10.1186/1758-2946-6-13>.
- [26] Z. Liu, F. Guo, Y. Wang, C. Li, X. Zhang, H. Li, L. Diao, J. Gu, W. Wang, D. Li, F. He, BATMAN-TCM: a bioinformatics analysis tool for molecular mechanism of traditional chinese medicine, Sci. Rep. 6 (2016) 21146, <https://doi.org/10.1038/srep21146>.
- [27] G. Stelzer, N. Rosen, I. Plaschkes, S. Zimmerman, M. Twik, S. Fishilevich, T.I. Stein, R. Nudel, I. Lieder, Y. Mazor, S. Kaplan, D. Dahary, D. Warshawsky, Y. Guan-Golan, A. Kohn, N. Rappaport, M. Safran, D. Lancet, The genecards suite: from gene data mining to disease genome sequence analyses, Curr. Protoc. Bioinforma. 54 (2016) 1301–13033, <https://doi.org/10.1002/cpbi.5>.
- [28] A.P. Davis, T.C. Wieggers, J. Wieggers, C.J. Grondin, R.J. Johnson, D. Sciaky, C. J. Mattingly, CTD Anatomy: analyzing chemical-induced phenotypes and exposures from an anatomical perspective, with implications for environmental health studies, Curr. Res. Toxicol. 2 (2021) 128–139, <https://doi.org/10.1016/j.crtox.2021.03.001>.
- [29] D. Szklarczyk, J.H. Morris, H. Cook, M. Kuhn, S. Wyder, M. Simonovic, A. Santos, N.T. Doncheva, A. Roth, P. Bork, L.J. Jensen, C. von Mering, The STRING database in 2017: quality-controlled protein-protein association networks, made broadly accessible, Nucleic Acids Res. 45 (2017) D362–D368, <https://doi.org/10.1093/nar/gkw937>.
- [30] W. Huang da, B.T. Sherman, R.A. Lempicki, Bioinformatics enrichment tools: paths toward the comprehensive functional analysis of large gene lists, Nucleic Acids Res. 37 (2009) 1–13, <https://doi.org/10.1093/nar/gkn923>.
- [31] M. Kohl, S. Wiese, B. Warscheid, Cytoscape: software for visualization and analysis of biological networks, Methods Mol. Biol. 696 (2011) 291–303, https://doi.org/10.1007/978-1-60761-987-1_18.
- [32] O. Trott, A.J. Olson, AutoDock Vina: improving the speed and accuracy of docking with a new scoring function, efficient optimization, and multithreading, J. Comput. Chem. 31 (2010) 455–461, <https://doi.org/10.1002/jcc.21334>.
- [33] J.T. Li, A.C. Melton, G. Su, D.E. Hamm, M. LaFemina, J. Howard, X. Fang, S. Bhat, K.M. Huynh, C.M. O’Kane, R.J. Ingram, R.R. Muir, D.F. McAuley, M.A. Matthay, D. Sheppard, Unexpected role for adaptive αTh17 cells in acute respiratory distress syndrome, J. Immunol. 195 (2015) 87–95, <https://doi.org/10.4049/jimmunol.1500054>.
- [34] L. Li, W.W. Fu, R.T. Wu, Y.H. Song, W.Y. Wu, S.H. Yin, W.J. Li, M.Y. Xie, Protective effect of Ganoderma atrum polysaccharides in acute lung injury rats and its metabolomics, Int. J. Biol. Macromol. 142 (2020) 693–704, <https://doi.org/10.1016/j.ijbiomac.2019.10.010>.
- [35] Y. Wang, X. Sang, R. Shao, H. Qin, X. Chen, Z. Xue, L. Li, Y. Wang, Y. Zhu, Y. Chang, X. Gao, B. Zhang, H. Zhang, J. Yang, Xuanfei Baidu Decoction protects against macrophages induced inflammation and pulmonary fibrosis via inhibiting IL-6/STAT3 signaling pathway, J. Ethnopharmacol. 283 (2021), 114701, <https://doi.org/10.1016/j.jep.2021.114701>.
- [36] X. Chen, J. Tang, W. Shuai, J. Meng, J. Feng, Z. Han, Macrophage polarization and its role in the pathogenesis of acute lung injury/acute respiratory distress syndrome, Inflamm. Res. 69 (2020) 883–895, <https://doi.org/10.1007/s00011-020-01378-2>.
- [37] W. Yao, X. Han, Y. Guan, J. Guan, S. Wu, C. Chen, H. Li, Z. Hei, Neutrophil Elastase Inhibitors Suppress Oxidative Stress in Lung during Liver Transplantation, Oxid. Med. Cell. Longev. DOI 10.1155/2019/7323986(2019) 7323986. <https://doi.org/10.1155/2019/7323986>.
- [38] Y. Jamilloux, T. Henry, A. Belot, S. Viel, M. Fauter, T. El Jammal, T. Walzer, B. Francois, P. Seve, Should we stimulate or suppress immune responses in COVID-19? Cytokine and anti-cytokine interventions, Autoimmun. Rev. 19 (2020), 102567, <https://doi.org/10.1016/j.autrev.2020.102567>.
- [39] B. Liu, M. Li, Z. Zhou, X. Guan, Y. Xiang, Can we use interleukin-6 (IL-6) blockade for coronavirus disease 2019 (COVID-19)-induced cytokine release syndrome (CRS)? J. Autoimmun. 111 (2020), 102452 <https://doi.org/10.1016/j.jaut.2020.102452>.
- [40] E. Mahase, Covid-19: Anti-TNF drug adalimumab to be trialled for patients in the community, BMJ 371 (2020) m3847, <https://doi.org/10.1136/bmj.m3847>.
- [41] F.R. D’Alessio, Mouse models of acute lung injury and ARDS, Methods Mol. Biol. 2018 (1809) 341–350, https://doi.org/10.1007/978-1-4939-8570-8_22.
- [42] M. Bosch, M. Sanchez-Alvarez, A. Fajardo, R. Kapetanovic, B. Steiner, F. Dutra, L. Moreira, J.A. Lopez, R. Campo, M. Mari, F. Morales-Paytuvia, O. Tort, A. Gubern, R.M. Templin, J.E.B. Curson, N. Martel, C. Catala, F. Lozano, F. Tebar, C. Enrich, J. Vazquez, M.A. Del Pozo, M.J. Sweet, P.T. Bozza, S.P. Gross, R.G. Parton, A. Pol, Mammalian lipid droplets are innate immune hubs integrating cell metabolism and host defense, Science 370 (2020), <https://doi.org/10.1126/science.aay8085>.
- [43] Z. Ding, R. Zhong, Y. Yang, T. Xia, W. Wang, Y. Wang, N. Xing, Y. Luo, S. Li, L. Shang, Z. Shu, Systems pharmacology reveals the mechanism of activity of Ge-Gen-Qin-Lian decoction against LPS-induced acute lung injury: a novel strategy for exploring active components and effective mechanism of TCM formulae, Pharmacol. Res. 156 (2020), 104759, <https://doi.org/10.1016/j.phrs.2020.104759>.
- [44] S.H. Kim, J.H. Hong, W.K. Yang, J.H. Geum, H.R. Kim, S.Y. Choi, Y.M. Kang, H. J. An, Y.C. Lee, Herbal combinational medication of glycyrrhiza glabra, agastache rugosa containing glycyrrhizic acid, tiliarin inhibits neutrophilic lung inflammation by affecting CXCL2, interleukin-17/STAT3 signal pathways in a murine model of COPD, Nutrients 12 (2020), <https://doi.org/10.3390/nu12040926>.
- [45] Q. Jiang, M. Yi, Q. Guo, C. Wang, H. Wang, S. Meng, C. Liu, Y. Fu, H. Ji, T. Chen, Protective effects of polydatin on lipopolysaccharide-induced acute lung injury through TLR4-MyD88-NF-κB pathway, Int. Immunopharmacol. 29 (2015) 370–376, <https://doi.org/10.1016/j.intimp.2015.10.027>.
- [46] Y. Zhang, D. Xu, H. Qi, Y. Yuan, H. Liu, S. Yao, S. Yuan, J. Zhang, Enriched environment promotes post-stroke neurogenesis through NF-κB-mediated secretion of IL-17A from astrocytes, Brain Res. 1687 (2018) 20–31, <https://doi.org/10.1016/j.brainres.2018.02.030>.
- [47] X. Li, C. Ye, M. Mulati, L. Sun, F. Qian, Ellipticine blocks synergistic effects of IL-17A and TNF-α in epithelial cells and alleviates acute pancreatitis-associated acute lung injury, Biochem. Pharmacol. 177 (2020), 113992, <https://doi.org/10.1016/j.bcp.2020.113992>.
- [48] M.J. McGeachy, D.J. Cua, S.L. Gaffen, The IL-17 family of cytokines in health and disease, Immunity 50 (2019) 892–906, <https://doi.org/10.1016/j.immuni.2019.03.021>.
- [49] Y. Xiong, Y. Liu, L. Cao, D. Wang, M. Guo, A. Jiang, D. Guo, W. Hu, J. Yang, Z. Tang, H. Wu, Y. Lin, M. Zhang, Q. Zhang, M. Shi, Y. Liu, Y. Zhou, K. Lan, Y. Chen, Transcriptomic characteristics of bronchoalveolar lavage fluid and peripheral blood mononuclear cells in COVID-19 patients, Emerg. Microbes Infect. 9 (2020) 761–770, <https://doi.org/10.1080/22221751.2020.1747363>.
- [50] H. Raghu, C.M. Lopus, Q. Wang, H.H. Wong, N. Lingampalli, F. Oliviero, L. Punzi, N.J. Giori, S.B. Goodman, C.R. Chu, J.B. Sokolove, W.H. Robinson, CCL2/CCR2, but not CCL5/CCR5, mediates monocyte recruitment, inflammation and cartilage destruction in osteoarthritis, Ann. Rheum. Dis. 76 (2017) 914–922, <https://doi.org/10.1136/annrheumdis-2016-210426>.
- [51] H. Shaath, R. Vishnubalaji, E. Elkord, N.M. Alajez, Single-cell transcriptome analysis highlights a role for neutrophils and inflammatory macrophages in the pathogenesis of severe COVID-19, Cells 9 (2020), <https://doi.org/10.3390/cells9112374>.
- [52] N. Izykowski, M. Kuehnelt, K. Hussein, K. Mitschke, M. Gunn, S. Janciauskiene, A. Haverich, G. Warnecke, F. Laenger, U. Maus, D. Jonigk, Organizing pneumonia in mice and men, J. Transl. Med. 14 (2016) 169, <https://doi.org/10.1186/s12967-016-0933-6>.
- [53] J. Hästbacka, R. Linko, T. Tervahartiala, T. Varpula, S. Hovilehto, I. Parviainen, S. T. Vaara, T. Sorsa, V. Pettilä, Serum MMP-8 and TIMP-1 in critically ill patients with acute respiratory failure: TIMP-1 is associated with increased 90-day mortality, Anesth. Analg. 118 (2014) 790–798, <https://doi.org/10.1213/ane.0000000000000120>.
- [54] S.F. Monaghan, R.K. Thakkar, D.S. Heffernan, X. Huang, C.S. Chung, J. Lomas-Neira, W.G. Cioffi, A. Ayala, Mechanisms of indirect acute lung injury: a novel role for the coinhibitory receptor, programmed death-1, Ann. Surg. 255 (2012) 158–164, <https://doi.org/10.1097/SLA.0b013e31823433ca>.
- [55] L.J. Celada, J.A. Kropski, J.D. Herazo-Maya, W. Luo, A. Greedy, A.T. Abad, O. S. Chioma, G. Lee, N.E. Hassell, G.I. Shaginurova, Y. Wang, J.E. Johnson, A. Kerrigan, W.R. Mason, R.P. Baughman, G.D. Ayers, G.R. Bernard, D.A. Culver, C. G. Montgomery, T.M. Maher, P.L. Molyneaux, I. Noth, S.E. Mutsaers, C.M. Prele, R. S. Peebles Jr., D.C. Newcomb, N. Kaminski, T.S. Blackwell, L. Van Kaer, W. P. Drake, PD-1 up-regulation on CD4(+) T cells promotes pulmonary fibrosis through STAT3-mediated IL-17A and TGF-β1 production, Sci. Transl. Med. 10 (2018), <https://doi.org/10.1126/scitranslmed.aar8356>.